T.R.
BOLU ABANT İZZET BAYSAL UNIVERSITY
INSTITUTE OF GRADUATE STUDIES
DEPARTMENT OF PHYSİCS

AB INITO CALCULATIONS ON PHYSICAL PROPERTIES OF CaB_2 IN THE AlB_2 STRUCTURE

MASTERS OF SCIENCE

NABEEL IBRAHIM AHMED AHMED

ACADEMIC SUPERVISOR
Prof. Dr. Cihan PARLAK

BOLU, DECEMER - 2022

APPROVAL OF THE THESIS

Ab inito Calculations on Physical Properties of CaB_2 in AlB_2 Structure submitted by **Nabeel Ibrahim Ahmed AHMED** and defended before the Examining Committe Members listed below in partial fulfillment of the requirements for the degree of **Master of Science** in **Department of Physics, Institute of Graduate Studies of Bolu Abant Izzet Baysal University in 23.12.2022 by.**

Examining Committee Members	**Signature**
Supervisor Prof. Dr. Cihan PARLAK Bolu Abant Izzet Baysal University	.....
Member Prof. Dr. Gürcan YILDIRIM Bolu Abant Izzet Baysal University	.....
Member Assoc. Prof. Dr. Yusuf ZALAOĞLU Osmaniye Korkut Ata University	.....

Prof. Dr. İbrahim KÜRTÜL
Director of Instıtute of Graduate Studies

ETHICAL DECLARATION

In this thesis dissertation that was properly prepared according to the Thesis Writing Rules of Bolu Abant İzzet Baysal University of the Institute of Graduates Studies, I hereby declare that;

- All data, information, and documents presented in the thesis were obtained in accordance with the academic and ethical rules,
- All data, documents, assessments, and results were presented in accordance with the scientific ethical and moral rules,
- All works that were benefitted in the thesis were appropriately cited,
- No alteration was made in the data used,
- Study presented in this thesis is original,

Otherwise, I declare that I accept the loss of all my rights in case any contradiction that may arise against me.

Based on the plagiarism report that was generated on the date of 29/12/2022 by using predetermined filtrations set by Directorate of Institute of Graduate Studies of the Turnitin programme, a plagiarism detection sofware, the similarity index detected was 25 %.

_____

Nabeel Ibrahim Ahmed AHMED

To the first teacher of humanity,

Our Noble Messenger MOHAMMED (peace be upon him)

To my mother (may God prolong her life)

To my dear daughters, Aseil, Retaj, Yaqeen

To my dear brothers and dear sisters

To my friends and colleagues

To every hand and heart that walked with me to achieve this achievement

I dedicate to you the fruit of my labors

ABSTRACT

AB INITO CALCULATIONS ON PHYSICAL PROPERTIES OF CaB_2 IN AlB_2 STRUCTURE
MSC THESIS
NABEEL IBRAHIM AHMED AHMED
BOLU ABANT IZZET BAYSAL UNIVERSITY
INSTITUTE OF GRADUATE STUDIES
DEPARTMENT OF PHYSICS
SUPERVISOR: PROF. DR. CIHAN PARLAK)

BOLU, DECEMBER 2022
(XV + 52)

We have studied in this thesis on the physical properties of CaB_2, in the AlB_2 structure. It is crucial to use first-principles calculation methods to determine the fundamental properties of materials as precise electronic and lattice dynamical features. By using the Density Functional Perturbation Theory (DFPT), elastic constants, phonon frequencies, and electron-phonon coupling (epc) properties of CaB_2 material, which are crucial for superconducting (SC) behaviour are calculated in this study. Also, we have used in all calculations both General Gradient Approximation (GGA) and Local Density Approximation (LDA), with a plane wave basis set. We have reported detailed calculation of the material's bulk modulus, bond lengths, and lattice constans. We calculated the topologies of the Fermi surfaces, the electron density of states, and compared them with MgB_2, an important superconductor in AlB_2 sturucture, discovered earlier in this regard.

Basic mechanical properties were calculated with the aid of elastic constants, such as Poisson's ratio, Young's modulus, Debye temperatures, etc. It was investigated whether there is a relationship between the determined parameters of the CaB_2 material and its superconducting properties. Calculations showed that phonon structures and electronic band structures have a close relationship with superconducting properties. The critical superconducting transition temperature (T_C) value is discovered to be 24.71/22.75 K (in GGA and LDA, respectively), using the Allen-Dynes.modified McMillan formulations.

KEYWORDS: Hexagonal CaB_2, Superconductivity, Ab inito calculations, Elastic properties, Electronic band structure, Electron-Phonon coupling.

ÖZET

AB INITO CALCULATIONS ON PHYSICAL PROPERTIES OF CaB_2 IN AlB_2 STRUCTURE
YÜKSEK LİSANS TEZİ
NABEEL IBRAHIM AHMED AHMED
BOLU ABANT İZZET BAYSAL ÜNİVERSİTESİ
LİSANSÜSTÜ EĞİTİM ENSTİTÜSÜ
FIZIK ANABİLİM DALI

(TEZ DANIŞMANI: PROF. DR. CIHAN PARLAK)

BOLU, EKİM - 2022
(XV+52)

Bu tezde, AlB_2 yapısındaki CaB_2'nin fiziksel özellikleri üzerinde çalıştık. Hassas elektronik ve örgü dinamiği özellikleri gibi malzemelerin temel özelliklerini belirlemek için temel ilkeler hesaplama yöntemlerini kullanmak çok önemlidir. Bu çalışmada, CaB_2 malzemesinin süperiletkenlik davranışı için çok önemli olan elastik sabitleri, fonon frekansları ve elektron-fonon eşleşme özellikleri Yoğunluk Fonksiyonel Pertürbasyon Teorisi (YFPT) kullanılarak hesaplanmıştır. Ayrıca tüm hesaplamalarda hem Genel Gradyan Yaklaşımını (GGY) hem de Yerel Yoğunluk Yaklaşımını (YYY) bir düzlem dalga temel seti ile kullanıldı. Malzemenin bulk modülü, bağ uzunlukları ve örgü sabitlerini ayrıntılı olarak rapor ettik. Fermi yüzey topolojilerini, elektron durum yoğunluğunu hesapladık ve bunları daha önce keşfedilen AlB_2 yapısında önemli bir süperiletken olan MgB_2 ile karşılaştırdık.

Elastik sabitler yardımıyla Poisson oranı, Young modülü, Debye sıcaklıkları gibi temel mekanik özellikler hesaplandı. CaB_2 malzemesinin belirlenen parametreleri ile süperiletkenlik özellikleri arasında bir ilişki olup olmadığı araştırıldı. Hesaplamalar, fonon yapılarının ve elektronik bant yapılarının süperiletken özelliklerle yakın bir ilişkisi olduğunu göstermiştir. Allen-Dynes modifiye McMillan formülasyonları kullanılarak kritik süperiletken geçiş sıcaklığı değerinin 24.71/22.75 K (sırasıyla GGA ve LDA'da) olduğu bulundu.

ANAHTAR KELİMELER: Altıgen CaB_2, Süperiletkenlik, Ab into hesaplamalar, Elastik özellikler, Elektronik bant yapısı, Elektron-Fonon eşleşmesi.

TABLE OF CONTENTS

LIST OF FIGURES

Page

LIST OF TABLES

Page

LIST OF ABBREVIATIONS AND SYMBOLS

DOS : Density of States

BZ : Brillouin Zone

μ* : coulomb pseudopotential

T_C : Superconducting Transition Temperature

eV : Electron Volt

Ha : Hartree

Å : Angstrom

B_o : Bulk Modulus

B',Bp : Pressure Derivative of Bulk Moduli

GPa : Gigapascal

EOS : Equation of State

Vo : EquilibriumVolume

au : Atomic unit

C_{ij} : Elastic tensor elements

B_V : Voigt Bulk Moduli

G_V : Voigt Shear Moduli

B_R : Reuss Bulk Moduli

G_R : Reuss Shear Moduli

G : Shear moduli

E : Young Modulus

H_v : Vickers hardness

A_u : Universal elastic anisotropy index

A : Zener anisotropy factor

β : Compressibility

θ_D : Debye Temperature

ω_{ln} : Logarithmic Average Frequency

ω : phonon frequency

λ : electron-phonon coupling constant

E_F : Fermi level

$N(E_F)$: Totalelectronic DOS at Fermi energy level

e-ph : Electron-phonon interaction

BCS : Bardeen-Cooper-Schrieffer theory

XC **:** Exchange-Correlation

ACKNOWLEDGEMENTS

The author wishes to express his deepest gratitude to his supervisor Prof. Dr. **CİHAN PARLAK** for his guidance, advice, criticism, encouragements, and insight throughout the research.

The author would also like to thank the soul of my honorable professor **Assoc. Prof. Dr. AMMAR AL- BATAWI**, (may Allah have mercy on him), who encouraged me a lot to complete my academic achievement. (Gratitude and Loyalty).

The some calculations reported in this study were performed at TUBITAK ULAKBIM High Performance and Grid Computing Center (TRUBA Resources).

1. INTRODUCTION

AlB_2 compound consists mainly of a simple form of only two elements, aluminum and bromine, and this compound is prepared from a direct interaction between the two elements in the presence of two main factors, namely, the vacuum and a temperature close to 800°C, and this compound is in the form of crystals with simple cubic (1).

$$Al + B_2 \rightarrow AlB_2$$

AlB_2- type materials have gained lots of attention from scientists with discovery of superconducting (SC) phenomena in the layered structure MgB_2 (39 K (2)). AlB_2-type structures dominate many current studies due to their better distinctive characteristics, including the electron-phonon (ep) pairing process (3) and electronic, SC and lattice dynamical properties (4). MgB_2 is an inorganic chemical compound that is found in nature in the form of a dark gray solid, it is an insoluble compound in water. It is of interest for many low-cost superconductivity applications (5).

The relatively high critical temperatures of the superconductor created an impossible challenge to its widespread adoption even when it showed considerable practical promise(6). The scientific community now views all AlB_2-type layered materials as being of utmost importance due to the finding of the superconducting MgB_2 molecule. In addition, several different alloys with high T_C, including alkaline-earth intercalated graphite's, share its hexagonal layered structure. Because they are comparable to MgB_2 superconducting material, hexagonal stacked materials with distinctive physical properties are of particular interest to researchers.

Our reason for choosing the CaB_2 material was that we thought CaB_2 would show a superconducting transition temperature like MgB_2, although it has not yet been synthesized. Although not experimentally observed, CaB_2 has been the subject of some theoretical studies (7) (8) (9) (10). We think that the main reason why AlB_2 phase was not obtained may be the predominance of the CaB_6 phase during the synthesis.

Choi *et. al.* (7) calculated lattice properties and superconducting characteristics of a hypothetical simple hexagonal CaB_2. They determined the specific heat, the Fermi surface superconducting energy gap, and superconducting transition temperature (T_C = 50.46° K) and compare them to the relevant MgB_2 parameters.

H.B. Ozisik *et.al.*(8) they studied have investigated the elastic, mechanical, and lattice dynamical characteristics of BeB_2, NaB_2, and CaB_2 compounds in AlB_2, OsB_2, and ReB_2 structures related to density functional theory. Exchange-correlation model has been utilized with generalized gradient approximation (GGA). Elastic constants, shear modulus, Bulk modulus, and Young modulus, additional factors include Poisson ratio, Debye temperature, sound velocities, and anisotropic factor calculated and discussed. Related phonon dispersion curves and DOS there is shown.

Shein *et.al.* (9) studied 18 hexagonal AlB_2-like diborides of *s, p,* and *d* metals subjected to FP-LAPW-GGA calculations to determine the systematic patterns for elastic characteristics. They reported the stable ones (MgB_2, AlB_2, ScB_2, YB_2, TiB_2, ZrB_2, HfB_2, VB_2, NbB_2, TaB_2 and CrB_2), the metastable ones (MoB_2, and WB_2), and speculative stages (NaB_2, BeB_2, CaB_2, AgB_2 and AuB_2). They discovered a collection of fundamental elastic properties of the MB_2-like ceramics as Bulk moduli (B), shear moduli (G), and Poisson ratio (ν) etc.

In this study, DFT, which has been extremely popular in materials science in the last two decades, is used DFT, described by explaining the electronic ground-state of a solid, typically, the total energy and electron density, is utilized to convert the many-body electron problem into a one-electron problem. From the total energy, many interesting Bulk physical of the material can be discovered by having some structural factors (11).

large category of alloys with high T_C shares the hexagonal layered structure, including ternary metallic materials and alkaline-earth intercalated graphite (10). MAB (M= Ca, Sr, Ba; A= Al, Ga, in; B = Si, Ge, Sn) materials. All the stacked hexagonal materials, each with a distinct physical property characteristic are seen to be a fascinating study topic because of their similarity to SC metal (MgB_2) (4). Because similarity of AlB_2 type CaB_2 and MgB_2, it's finding their SC qualities is an

intriguing area of research. This study aims to examine all characteristics of the CaB_2 structure, including elastic properties, superconducting behavior, and electronic band structures, as well as to investigate its detailed basic physical features of it.

Computational superconductivity gets dense attention because of recent notable developments in first principles calculations that have successfully led to several prospective future discoveries. This method's novel benefit is that it dispenses with costly tests and enables the creation of superconducting materials and calculating and finding their outcomes. For the discovery of new superconductors computational superconductivity is a highly effective tool Ref. (6).

The plan of this thesis is as follows: in the introduction part of this study, a brief presentation was made about why we chose the CaB_2 material as the study subject and the methods used in this study and the results to be obtained. In chapter two shows a concise information about the theoretical approaches used in this study. We have used the definition of computational physics, as well as discussed about superconductivity and its relationship to DFT, moreover, provided a brief explanation of DFT core concepts in context of pseudopotential plane-wave implementation. Regarding chapter three, the calculations discussed in this study and previous calculations are given. In this section, electronic structures, phonon structures and superconducting properties are discussed in detail. The thesis end with a brief overview of the results in Chapter four.

2. THEORETICAL BACKGROUND

In this chapter we first define superconductivity (SC), we mentioned the most important elements in SC, and we talked about the most important applications of SC. In the next part, we spoke about computational physics, and density functional theory, and explained its mechanisms. We also talked about computational superconductivity, as we mentioned the equations related to our study.

2.1 Superconductivity

It is the ability of some materials to transfer electricity with essentially no known resistance. This ability has intriguing and maybe beneficial ramifications. Generally, low temperatures are necessary for a material to exhibit superconductor behavior.

The first instance of SC was discovered in 1911 by Dutch scientist H. K. Onnes. The temperature of liquid helium, 4° K , was used in his experiment with elemental mercury. The perfect material one that can superconduct at ambient temperature remains elusive, however, certain compounds have since been created to function as superconductors at higher temperatures.

The detection of room-temperature SC is one of the long-standing problems in experimental physics (12). A material that shows operating temperatures above 0 °C (273 K, 32 °F) for SC, or temperatures that are readily attained and sustained in an everyday setting, is known as a room-temperature superconductor. Heavily compressed carbon sulfur hydride has the highest allowable temperature for SC as of 2020. With a crucial transition temperature of +15°C at 267 GPa (13).

Physics was significantly impacted by the 1986 discovery that a copper oxide compound could superconduct at a temperature greater than any material at the time. The material, created by chemically doping the oxide La_2CuO_4, showed SC at about 30 K, according to reports by George Bednorz and Karl Muller (14).

The conductor is niobium-titanium (NbTi), which is superconductive below 9.4 °K. utilized in almost every modern superconducting MR scanner. Each wire consists of many NbTi microfilaments enclosed in a copper core. the tiny

microfilaments are supported and protected by the copper core, which also serves as a low resistance channel for big currents in the case that SC is lost. Due to its significantly higher transition temperature (39°K), MgB_2 is a unique superconducting material that is increasingly being employed in scanners and other magnetic devices.

With the invention of MRI equipment, superconductors have already profou ndly altered the field of medicine and resulted in a decline in exploratory surgery. Superconductors are utilized to create incredibly strong electromagnets that rapidly accelerate charged particles (close to the speed of light). also, superconducting Quantum Interference Devices. they aid in the detonation of land mines by being utilized in mine detecting devices. The superconducting single-photon detector, superconducting tunnel junction detector, superconducting strain gauge, and kinetic induction detectors are only a few of the high sensitivity particle detectors that utilize them. Scientific magnets with a high field also employ superconductors. without the need for rockets, satellites may be launched into orbit from the Earth using superconducting magnetic propulsion systems. Superconducting magnets may be utilized to construct high-efficiency separators that can be used to separate malignant cells from healthy cells utilizing a high-gradient magnetic separation technique. A superconducting wire can be utilized for transmission lines since the current can pass through it without changing in size.

Other superconductor-related effects Finding superconductors that work at temperatures far higher than those now known will depend on technology, or on finding less expensive means to achieve the extremely low temperatures currently required to make them function. By using a wind-and-react technique, helical windings of Fe-sheathed MgB_2 wires of various diameters were created. The powder-in-tube (PIT) technique and ultra-fine starting precursors were used to create wires with a 1 mm2 cross-section and a 20% superconductor core (5).

2.2 Computational Physics

Computational physics is a discipline of theoretical physics that is primarily centered on the study and application of algorithms to physical issues based on scientifically proven physics. Where it implements numerical analysis to solve problems in physics that are related to complex quantum theories, and it saves us effort, time, and cost. Finite element techniques, Boltzmann network simulations, DFT, quantum particle dynamics, Monte Carlo simulations, and the title of one-dimensional quantum systems have all received new sections. But what concerns us in this post is DFT.

Ab Initio a phrase that means "from ancient or first" and is widely used in science It is employed in several contexts, the most significant of which are: In chemistry and physics, we may determine from the start if anything depends on the fundamental rules of nature without making any additional model-imposed assumptions. The values of the basic physical constants are the only starting inputs used in these computations (15).

In general, computational physics difficulties are highly challenging to resolve. This is due to several (mathematical) factors, including complexity, chaos, and a lack of algebraic or analytical solvability. For instance, it may take a lot of labor to create a workable algorithm for even seemingly straightforward issues, such as computing the wave function of an electron circling an atom under a strong electric field (16).

Finally, it might be challenging to assure that there are no numerical mistakes that become so significant that the "solution" becomes meaningless because many physical systems are, at best, chaotic and, at worst, nonlinear (17).

2.3 Density function theory (DFT)

It's the most important method used in theoretical physics by which we can determine the properties of a multi-particle system in all its details and find the system's total energy as well as the electronic density of orbitals, as well as the physical and optical parameters of matter), it's one of the most used theories in quantum computations, this is due to the ability to be easily applied to various systems at low cost and high speed. DFT is utilized often to determine the ground-state characteristics of atoms, molecules, solids, and other many-electron systems (18).

The difference between DFT and the old traditional methods is that the mechanism of these methods depends on its solution to the Schrödinger equation for a particular system composed of several atoms, as is the case in the Hartree-Fock theory and the methods inspired by it on the wave function with 3N variable (N represents total number of particles of system) And these are the reasons why these equations to be solved are complex and it requires a lot of effort and concentration. As for the DFT theory, the calculations are smooth and do not need a long time or high effort.

Based on various theoretical approaches to SC that primarily concentrate on the generic description of the phenomena, such as DFT and its expansions. The following are some of the usual issues that computational SC addresses:

1. What characteristics distinguish a certain substance from a lousy SC?
2. How are its characteristics affected by outside factors like doping, pressure, and strain?
3. Is it conceivable to develop new materials that outperform current ones in terms of their superconducting abilities?

The most important factor that determines a superconductor's performance for large-scale applications is its critical temperature, or T_C, so answering the questions above calls for the creation of techniques that are precise enough to predict a SC T_C and its dependence on external factors (6).

The main objective of DFT is to replace the wave function with the density function that contains three variables to be the basis for all the calculations. For this reason, dealing with DFT as a mathematical concept or as a physical concept is simplified and easy for researchers. DFT principle is to reformulate quantum problems and transform them from a problem into a complex multi-particle system. to a simplified one-gross issue.

When electrons and nuclei interact with one another through coulombic (electrostatic) forces, a system is said to be solid. The first finding is that nuclei move over time at a far slower rate than electrons do, and their mass is significantly more than that of electrons. This discovery can lead to what is known as "adiabatic approximation," which is the entanglement of nuclear degrees of freedom. Since the nuclei are assumed to be stationary in this approximation, the issue may be split into two parts: the problem of electrons and the problem of moving nuclei on a potential energy surface. While the answer to the second problem is the crystal's vibrational qualities, the first problem's solution would reveal the crystal's electronic energy band structure and electronic wave functions (19).

The total ground state energy might be minimized to calculate the ground state density. The ground state density might be calculated by minimizing this reduction concerning the single-particle wave function ψi(r) with the orthogonality constraint. Total energy at the ground state. This reduction is the only one compared to the orthogonality requirement on the single-particle wave function ψi(r).

$$< \psi_i \psi_j >= \delta_{ij} \qquad (1)$$

This in turn leads to Cohn-Sham equations.

$$\left[-\frac{1}{2m_e} \nabla^2 + V_H(\bar{r}) + V_{xc}(\bar{r}) + V_{ext}(\bar{r}) \right] \psi_i(\bar{r}) = \epsilon_{ij}\, \psi_i(\bar{r}) \qquad (2)$$

This equation solutions have been used to create charge density:

$$V_H(\bar{r}) = e^2 \int_V d\bar{r}_i \frac{n(\bar{r}_i)}{|\bar{r} - \bar{r}1|} \qquad (3)$$

Some of the most accurate tests of the theory of relativity have been made using Quantum-mechanical principles, or Hamiltonians, for determining the total energy of basic one-atom systems theory, as well as the formulas used to calculate the energies of more Complex systems are easy expansions of basic systems of these Hamiltonians for the atoms. Therefore, it is Reasonably anticipated quantum physics' predictive power. Precisely the total energies of atom groupings and this anticipation has so far been confirmed each time. Py repeated experimentation (20).

These strategies can help a wide spectrum of scientists, such as chemists, biologists, and geophysicists. It is frequently recommended that quantum. The primary purpose of mechanics was to describe occurrences on the issue of whether atomic scale "What value do computations involving quantum mechanics in a science that is unrelated directly with atomic-scale events. Since The interactions that make up and determine our reality of the details and fundamentals of atoms and molecules the last resting place of the world must be figuring out these interconnections.

Modern methods for solving the Schrodinger equation precisely determine the energy of covalent bonds as well as their polarizabilities, equilibrium lengths, and force constants. Physicalists have created many techniques that might be utilized to determine many different physical characteristics of elastic constants and lattice constants are examples of materials. These techniques, which merely call for a description of the ions are typically referred to as (by their atomic number) ab initio techniques numerous ab initio techniques used by physicists and chemists have been around for over ten years, every Ab initio over the past few years, techniques have been improved regularly.

The approach could only model few-atom systems. but now, this technique can simulate a thousand atoms. Systems and that much is already obvious. Expanding the realm of quantum mechanics to the degree that modeling goes, the total-energy pseudopotential approach makes a variety of intriguing issues possible. computation using quantum mechanics, and the future provide numerous new applications for quantum mechanics scientific disciplines More atoms are present due to this. It's directly attributable to an increase in processing power of the ab initio pseudopotential's effectiveness approach, which implies that more people are

using it. class of issues where using it is more cost-effective experiment than quantum-mechanical modeling to ascertain systems' physical characteristics (20).

2.4 Computational Superconductivity

The rapid development and widespread implementation of Ab-initio techniques transformed them from helpful tools for interpreting current superconductors to reliable forecasting tools for emerging superconductors in less than 20 years. The Bardeen-Cooper-Schrieffer (BCS) theory, the most basic microscopic theory of SC, describes the superconducting state as a state of macroscopic quantum coherence in which electrons pair up into Cooper Pairs with opposing spin and momentum and are held together by an attractive glue. This adhesive is now referred to as lattice vibrations (phonons). Furthermore, diagrammatic theory for interacting electrons and bosons is known as the Migdal-Eliashberg theory. It's a strong-coupling extension of BCS theory the foundation of the theory is the so-called (isotropic) electron-phonon spectral function, and it's defined as:

$$\alpha^2 \mathrm{F}(\omega) = \left[\frac{1}{N(E_F)} \sum_{kq.v} \lceil \mathrm{g} \mathrm{k}_1 \mathrm{k} + \mathrm{q}, \mathrm{v} \rceil \right]^2 \delta(\varepsilon_k^n)\, \delta(\varepsilon_{k+q}^m)\, \delta(\omega - \omega_{q,v}) \qquad (4)$$

where $N(E_F)$ is the DOS at the Fermi level, $\omega q,v$ is the phonon frequency of mode υ and wave vector q, and $\lceil g, k_1 k + q, v \rceil$ gis the e-ph matrix component at the Fermi level between the two electronic states of wave vectors k and k + q. The e-ph spectral function equation $\alpha^2 f(\omega)$ provides evidence for why SC qualities are difficult to anticipate. Are so sensitive to small details of the electronic structure of a given material): since in Eq. (1) the phonon spectrum is weighted by the e-ph matrix elements $\lceil g,k+q,v \rceil$, which can be very different for different phonon modes, and since the double delta function $\delta(\varepsilon_k^n)\, \delta(\varepsilon_{k+q}^m)$ just a small portion of the whole electronic and photonic spectrum contributes to SC, which limits the sum of the e-ph matrix components to electronic states at the Fermi level.

Understanding and predicting new conventional superconductors essentially involves explaining or conceiving materials where electrons and phonons are strongly coupled (large $\lceil g, k_1 k + q, v \rceil$), which can be done with a high degree of accuracy because all variables that enter the e-ph spectral function can be

computed using density functional perturbation theory from the beginning. The critical temperature of a material may be calculated to various degrees of sophistication if the e-ph spectral function is known. The simplest method uses a rough formula for T_C; for phonon-mediated superconductors, the McMillan-Allen-Dynes formula is a popular option.

The superconducting transition temperature T_C has been calculated using Allen-Dynes modified McMillen equation as

$$T_C = \frac{\omega_{ln}}{1.2}\left[-\frac{1.04\,(1+\lambda)}{\lambda-\mu^*\,(1+0.62\,\lambda)}\right] \qquad (5)$$

where ω_{ln} indicates the logarithmic average frequency and μ* is the coulomb pseudopotential. The logarithmic average frequency calculated as

$$\omega_{ln} = \exp\left(\frac{2}{\lambda}\int_0^\infty d\omega\ \frac{\alpha^2 F(\omega)}{\omega}\ In\ \omega\right) \qquad (6)$$

$$\lambda = 2\int_2^\infty d\omega\ \frac{\alpha^2\,F\,(\omega)}{\omega} \qquad (7)$$

is the electron-phonon coupling constant (21).

2.5 The Pseudopotential Approximation

The pseudopotential approximation, first proposed by Hans G. A. Hellmann in 1934, is reviewed briefly as one of the most effective theories for computations of electronic structures. Recent advances in relativistic quantum theory make it possible to accurately adjust pseudopotential parameters to valence spectra, leading to results for the properties of atoms, molecules, and the solid state that, if a small-core definition is used, are in excellent agreement with more precise all-electron results. As a result, for systems including heavy elements, the relativistic pseudopotential approximation is now the technique that is used the most (22).

2.5.1 Local Density Approximation (LDA)

It approximates foundations according to the homogeneous gas model of the electron of which contains the closest concept that is explained by simplifying the exchange-correlation energy. However, the electron density of a heterogeneous gas can be considered locally homogeneous (23). The electronic density value at each location in space is the only factor influencing a set of exchange-correlation (XC) procedures for the energy functional in DFT known as LDA.

$$E_{XC}^{LDA}[\rho] = \int \rho(\vec{r})\varepsilon_{XC}\big(\rho(\vec{r})\big)d\vec{r} \qquad (8)$$

where ρ is the electronic density and εxc is the exchange-correlation energy per particle of a homogeneous electron gas of charge density ρ. The exchange-correlation energy is decomposed into exchange and correlation terms linearly. Ex is the electron exchange term and Ec is the electron correlation term. How one electron in an atom interacts with another is the subject of the electron correlation concept. The word "electron exchange" refers to the transfer of fermionic and bosonic electrons.

2.5.2 General Gradient Approximation (GGA)

It is an approximation that takes into consideration gradient-induced inhomogeneity of electrical density. In the GGA approximation, which is a correction to the LDA approximation, the exchange-correlation energy is linked to both the local electron density and the gradient of the electron density (23). Energy barriers, structural energy differences, total energies, atomization energies, and all of these tend to improve. Enlargement, fusion, and softening GGA Semiempirical GGA can be effective for tiny compounds (18). Results obtained by using the GGA functionals for band structure were considerably.

$$E_{XC}^{GGA}[\rho(\vec{r})] = \int \rho(\vec{r})\varepsilon_{XC}\big(\rho(\vec{r}), \nabla\rho(\vec{r})\big)d\vec{r} \qquad (9)$$

3. RESULTS

3.1 Methodology

All the calculations reported in this thesis were obtained by using ABINIT package (24). Which is an implementation of density functional theory (DFT) and uses a plane-wave basis for representing electronic wavefunctions. We used both local density approximation (LDA) and general gradient approximation (GGA) exchange correlation energy when doing all our calculations. The electron–ion interactions are accounted for by using norm conserving optimized pseudo-potentials produced by means of Opium code for LDA-Exc (25). The valence configurations for the construction of pseudopotentials are chosen as Ca ($3s^2 3p^6 3d^0 4s^0$), B ($2s^2 2p^{1.2}$). The GGA pseudo potentials taken from PseusoDojo project (26).

As is known, the calculation of vibrational properties and superconducting properties requires well converged total energies with regard to the influence of different K-point sampling and plane-wave cut-off energy. Thus, a series of test calculations are performed to find meV level convergence as can be seen in Table3.1.-Table3.4., Fig.3.1.-Fig.3.4. for LDA and GGA exchange-correlation. It is found that 40 Ha cut-off energy and 16x16x16 k-grid are required to achieve convergence at the meV level.

Table 3.1. Dependence of total energy on energy cut-off and energy differences for GGA-Exc.

Energy Cut-off (Ha)	Total Energy (Ha)	$\|\Delta E\|$ (eV)
25	−44.6075469	-
30	−44.6109656	0.09298860
35	−44.6115974	0.01718496
40	−44.6116898	0.00251328
45	−44.6116976	0.00021216

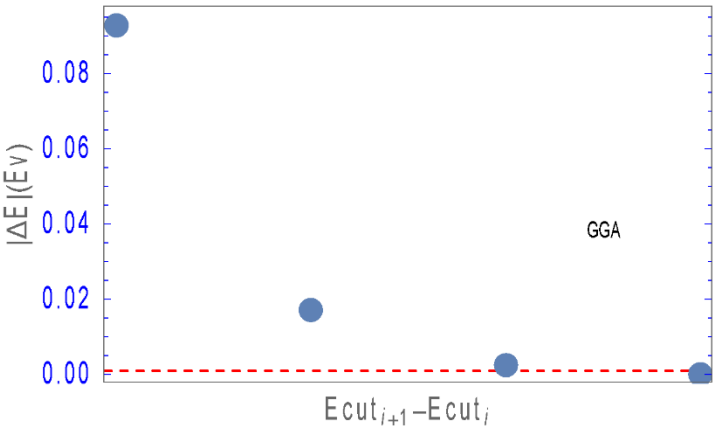

Figure 3.1. Differences in total energy for between Cut-off energy 25,30,35,40, and 45 Hartree (The data given in Table 3.1.).

Table 3.2 Dependence of total energy on k-grid and energy differences for GGA-Exc.

k-grid	Total Energy (Ha)	|ΔE| (eV)
10x10x10	−44.6116288	-
12x12x12	−44.6116492	0.0005553
14x14x14	−44.6117097	0.0016432
16x16x16	−44.6116898	0.0005411
18x18x18	−44.6116823	0.0002048

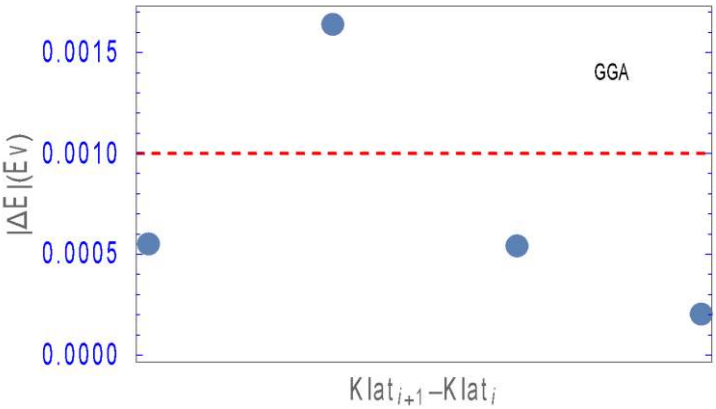

Figure 3.2. Difference in total energy for between k-grid 10x10x10, 12x12x12, 14x14x14, 16x16x16, and 18x18x18. (The data given in Table 3.2.).

Table 3.3. Dependence of total energy on energy cut-off and energy differences for for LDA-Exc.

Energy Cut-off (Ha)	Total Energy (Ha)	|ΔE| (eV)
25	−42.4541813	-
30	−42.4544578	0.0075208
35	−42.4544982	0.0010989
40	−42.4545434	0.0012294
45	−42.4545667	0.0006338

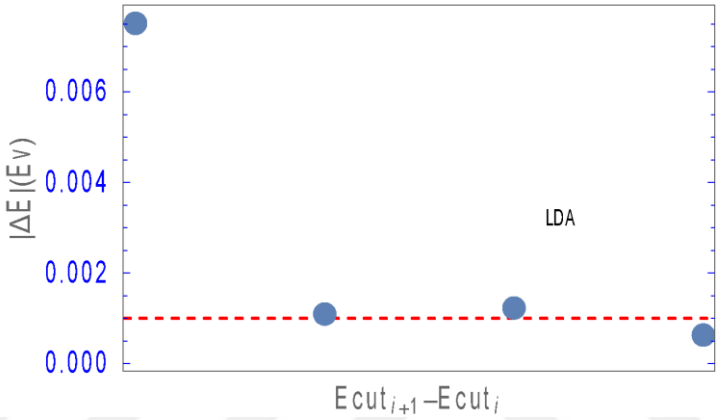

Figure 3.3. Total Energy difference for between cut-off energies 25,30,35,40 and 45 Hartree. (The data given in Table 3.3.).

Table 3.4. Dependence of total energy on k-grid and energy differences for LDA-Exc.

k-grid	Total Energy (Ha)	|ΔE| (eV)
10x10x10	−42.4544928	-
12x12x12	−42.4545131	0.0005536
14x14x14	−42.4545665	0.0014489
16x16x16	−42.4545434	0.0006262
18x18x18	−42.4545387	0.0001299

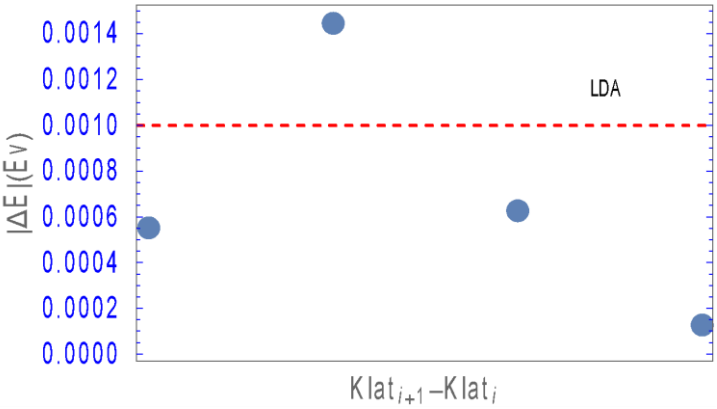

Figure 3.4. Total Energy difference for between k-grid 10x10x10, 12x12x12, 14x14x14, 16x16x16, and 18x18x18. (The data given in Table 3.4.).

3.2 Atomic Structure and Lattice Properties

Hypothetical AlB_2-type CaB_2, crystal has a well-known structure and composition (space group no: 191, P6/mmm, Z=1) (4). This structure is given in Fig. 3.5 and Fig.3.6, the B atoms are located at a hexagonal lattice between the Ca atoms layers. The boron atoms are arranged in hexagonal corners, with three boron atoms in each plane. The Ca atoms, on the other hand, are positioned in the center of each boron hexagon, but in the middle of consecutive boron layers, with each Ca atom having 12 nearest-neighbor B atoms and six nearest-neighbor in-plane Ca atoms (7). CaB_2 has the exact same symmetry as MgB_2, with one Ca and two B atoms in each unit cell.

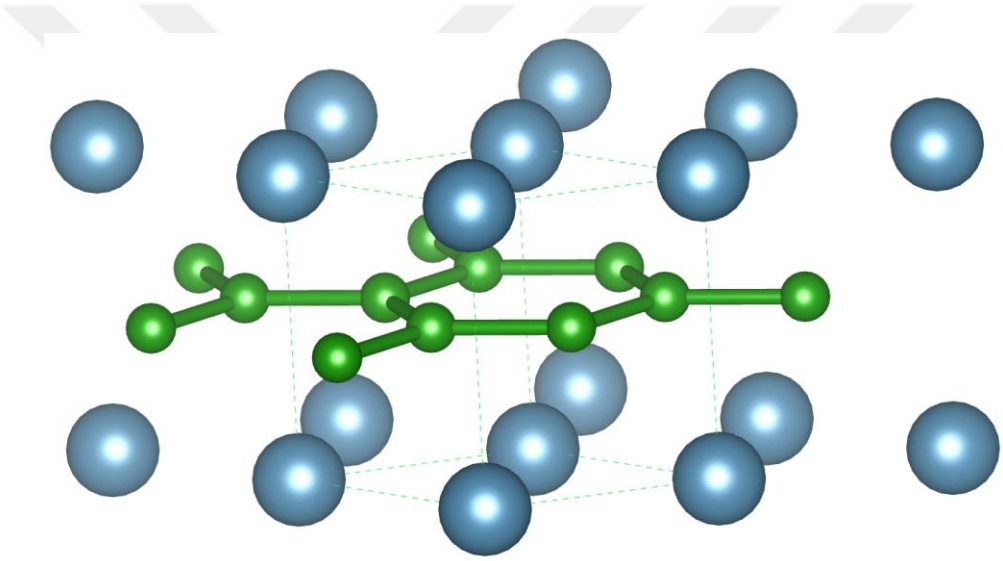

Figure 3.5. CaB_2 lattice structure, view from the xy-plane, green color represents B atoms, the blue color represents Ca atoms.

Wyckoff position is defined as a point belonging to a group of crystals that represents the position symmetry groups associated with the space group, where Wyckoff's positions give us the locations of the different space groups by which we can find any position relative to any point in a unit cell, Wyckoff position is defined as a point belonging to a group of crystal that represents the position symmetry groups associated with the space group, points were also utilized for compounds Ca-1a (0,0,0) and B-2d (1/3,2/3,1/2) (27).

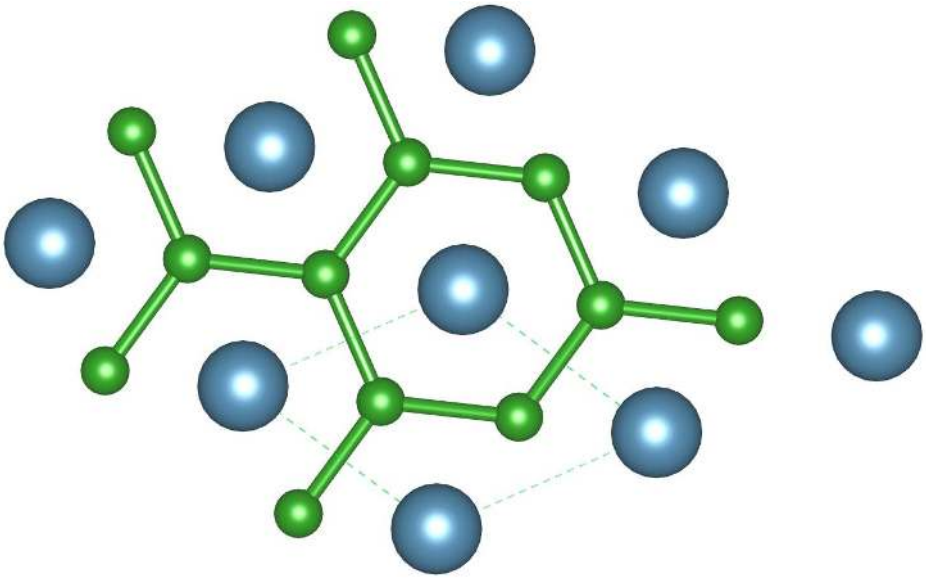

Figure 3.6. View of the CaB_2 lattice structure from the top.

Our calculated lattice parameters are given in Table 3.5. We found the values of *a* and *c* lattice parameters (3.171 Å, 4.003 Å (LDA)) which are completely identical to the values of *a* and *c* parameters of Ref. (28). On the other hand, the values of lattice constants *a* = 3.217 Å and *c* = 4.071 Å in GGA-Exc. Are in good agreement with the *a* and *c* values given in Ref. (29), (8), (30), (31), (7). We noticed that the values of *a* and *c* reduce while changing from GGA to LDA. In general, the optimized lattice constants are estimated to be slightly smaller than the experimental ones because of the usual LDA-over binding effect.

Table 3.5. Structural parameters (in Å), Bulk Modulus (B_o in GPa), pressure derivative of bulk modulus (B') and bond distance values (d in Å) of CaB_2.

Lat. Param.		This Work	(29)	(8)	(9)	(28)	(30)	(31)	(7)
LDA	a	3.171				3.183			3.185
	c	4.003				4.001			4.060
GGA	a	3.217	3.226	3.241	3.191		3.205	3.264	
	c	4.071	4.067	4.099	4.051		3.974	4.137	
LDA	d_{B-B}	1.831							
	d_{B-Ca}	2.713							
	d_{Ca-Ca}	3.171							
	B_o	133.9				141			
	B'	3.78							
GGA	d_{B-B}	1.857	1.863						
	d_{B-Ca}	2.756	2.758						
	d_{Ca-Ca}	3.217	3.226						
	B_o	121.6	121	120.7	122.2				
	B'	3.78		3.487					

Our calculated bond length values (in GGA) are also given in Table.3.5. All the values given in this section are very compatible with the values given in Ref. (29).

The important mechanical parameter, bulk modulus describes how resistance a substance exhibits under pressure. The Vinet EOS (32) can be used to calculate bulk modulus:

$$E_{(V)}=E_o+9B_oV_o\,(e^{A(1-x)}\,[A^{-1}(1-x)-A^{-2}]+A^{-2}) \qquad (10)$$

where V_o is the volume of equilibrium, $x=(V_o/V)^{1/3}$, B_o is Bulk Modulus,

$A=\frac{(3Bo'-1)}{2}$ and B_O' is pressure derivative of bulk modulus.

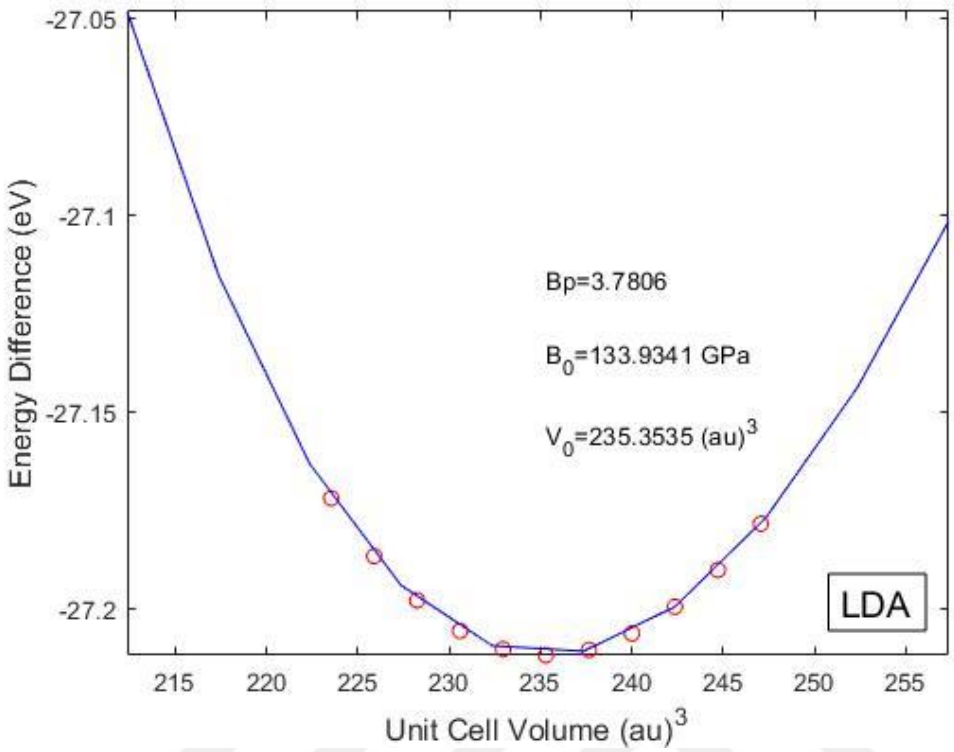

Figure 3.7. Total energy difference as a function of cell volume, solid line is the fits to the Vinet EOS.

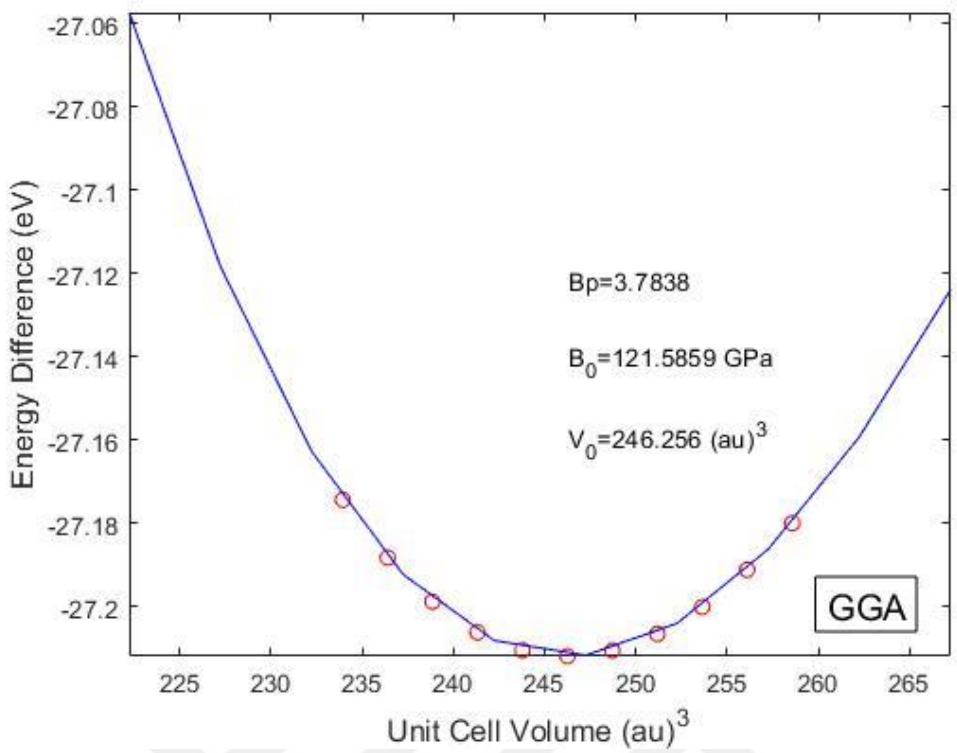

Figure 3.8. Total energy difference as a function of cell volume, solid line is the fits to the Vinet EOS.

Our calculated Bulk Modulus values from direct fit to a Vinet-EOS to be (B=133.9 GPa, B`= 3.780 (LDA) and B=121.6 GPa, B`= 3.783 (GGA)) given in Fig.3.7 and Fig.3.8. The values we calculated in GGA-Exc are very compatible with the literature data. There is a difference of 2 GPa between our LDA calculation and Ref.(28). This is an acceptable situation that may arise from the calculation parameters.

3.3 Elastic Properties

The widely used method for calculating the elastic constants of any material from first principles involves forcing the crystal to deform from its equilibrium shape through a series of quaternary deformations, as well as shearing of various sizes until the resulting stress can be easily calculated using the quantum mechanical definition of stress (15). The link between the components of applied

stress and computed stress yields a collection of hyper-defined linear equations that can be solved by decomposing a single value to get the elastic stiffness constants we want. Hamann et. al. (33) recently proposed a reduced-coordinate metric tensor approach for expressing a linear response to stress-type perturbations that may be estimated using density functional perturbation theory (DFPT). The reference approach, as implemented in ABINIT, is also used to get the elastic constants reported in this study (25).

For AlB_2- type (hexagonal) compounds, we identified six major components of elastic tensor (***C_{11}, C_{12}, C_{13}, C_{33}, C_{44},*** and ***C_{66}*** arranged in Young notation). Due to the material's space group symmetry properties (34), the related matrix is limited to six tensor elements. Our recognized Born stability criteria must be met for the elastic constants of hexagonal crystals, as well as the constants calculated in this message, and meet the following conditions (35):

$$C_{11} > 0,$$

$$C_{11}\text{-}C_{12} > 0,$$

$$(C_{11} + C_{12})\, C_{33}\text{-}2\, C_{13}^2 > 0.$$

Both LDA and GGA calculations that we make, meet these requirements. Mechanical stability is an important parameter for industrial use of a material. Calculated elastic constants enable us to obtain the macroscopic mechanical parameters of this material, the equations can indeed be calculated with the help of prime estimation of Voigt-Reuss-Hill (36), namely the bulk modulus (B), which is the precise measurement of how the crystal structure behaves to volume change under the applied load, and shear modulus (G), which is the measure of its ability of the material to resist transverse deformations. As functions of elastic constants, we might determine the Voigt bulk modulus (B_V) and the shear modulus (G_V):

$$B_V = \frac{1}{9}\,[2(C_{11}+C_{12}) + 4C_{13}+C_{33}] \qquad (11)$$

$$G_V = \frac{1}{30}\,(M + 12\,C_{44} + 12\,C_{66}] \qquad (12)$$

The Reuss bulk modulus (B_R) and shear modulus (G_R) are both defined as

$$B_R = \frac{C^2}{M} \qquad (13)$$

$$G_R = \frac{5}{2}\left[\frac{C^2 C_{44} C_{66}}{3B_V C_{44} C_{66} + C^2 (C_{44}+C_{66})}\right] \quad (14)$$

where C^2 and M given as:

$$C^2 = (C_{11}+C_{12})\, C_{33} - 2C_{13}^2 \quad (15)$$

$$M = C_{11}+C_{12}+2C_{33} - 4C_{13} \quad (16)$$

The elastic constant tensor, as well as the bulk and shear moduli, provide information on a material's hardness in comparison to other forms of deformation. The bulk and shear modulus can perhaps be better determined using average of the Reuss and Voigt coefficients:

$$B = \frac{B_V + B_R}{2} \quad (17)$$

$$G = \frac{G_V + G_R}{2} \quad (18)$$

We can calculate the Young modulus by using equation:

$$E = \frac{9BG}{3B+G} \quad (19)$$

Table 3.6. Calculated elastic constants (Cij in GPa).

Elas.Cons.	Pre. Work (LDA)	Pre. Work (GGA)	(8)	(9)	(29)	(31)
C_{11}	296.6	276.2	291.1	237.5	285	269
C_{12}	63.2	53.5	50.2	97.2	55	65
C_{13}	46.7	36.7	39.1	34.9	35	38
C_{33}	290.2	269.5	280.1	289.8	266	269
C_{44}	102.8	92.7	95.1	96.9	92	93
C_{66}	116.5	110.1	120.4		115	

Table 3.7 shows the macroscopic mechanical properties that we can calculate from the elastic constants. If we compare the bulk modulus values that we calculated by directly fitting the energy (B=133.9 GPa (LDA) and B=121.6 GPa, (GGA) with bulk modulus values we obtained from elastic constants (B=132.9 GPa, (LDA) and B=119.4 GPa, (GGA), we see that the values calculated for both exchange-correlation energies are compatible. These values can be seen to be quite low when we compare the bulk modulus of MB_2 with 161.6 GPa (37).

Table 3.7: Bulk (B), shear (G), Young (E) moduli, compressibility (β, in GPa^{-1}), Pugh's indices (G/B), Poisson's ratio (υ), Zener anisotropy factor (A), Universal elastic anisotropy index (A^u), and Vickers hardness (H_υ) in GPa are all calculated.

Values	Pre.Work (LDA)	Pre.Work (GGA)	(8)	(29)	(9)	(31)
B_V	132.9	119.5		121		
G_V	112.8	105.2		107		
B_R	132.8	119.3		120		
G_R	112.1	104.0		105		
B	132.9	119.4	124.2	121	122.2	121
G	112.5	104.6	110.2	106	111.5	
E	263.2	242.9	255.1		210.7	250
υ	0.1700	0.1610	0.1576	0.16	0.185	
A	0.88	0.83	0.77	0.08	1.22	
G/B	0.84	0.87	0.89		0.91	
H_v	23.1	23.0				
H_v^t	32.4	29.5				
A^u	0.03	0.06				
θ_D	902.8	867.3	894.6			

[t]Louie formulation (38)

The Zener anisotropy factor (A) can be calculated using the following equation:

$$A = \frac{2C_{44}}{C_{11} - C_{12}} \qquad (20)$$

if the A value is close to 1, elastic isotropy can be said to exist. Our results (0.88, 0.83) are relatively close to unity. Another isotropy formula for locally isotropic single crystals is the universal elastic anisotropy index (A^u) given as:

$$A^u = 5\frac{G_V}{G_R} + \frac{B_V}{B_R} \geq 0 \; . \qquad (21)$$

A^u For locally isotropic single crystals, is exactly zero. The single-crystal anisotropy's degree is determined by the divergence from zero. (39). Our calculated universal elastic anisotropy indexes are A^u=0.03 in LDA-Exc. and A^u=0.06 in GGA-Exc. In both calculations, the values are very near zero. The partially different results between A and A^u may be due to the fact that the Zener anisotropy formula contains only 3 elastic constants and restricted information about the other elastic constant (4).

Poisson's ratio ($\upsilon = \frac{(3B-2G)}{2(3B+G)}$) determines whether the material is compressible or incompressible. In nature, it ranges from 0 to 0.5 for most materials. The threshold value for ductile behavior is ≈0.25. In our calculations, the Poisson's ratio was determined to be 0.1700 (LDA) and 0.1610 (GGA). It is seen that these values are lower than the Threshold value of 0.25 and this value is very close to the value of Ref. (8) that is 0.1576. When we compare it with the value of MgB_2 (0.19 (40)), it is seen that the values obtained for CaB_2 are slightly lower. In addition, Pugh indices, which can be used to describe the ductility or brittleness of the material, were calculated in this study. In more detail, the ratio G/B>0.5 is directly related to the fragility nature of a material. Pugh indices for CaB_2 is 0.84 for LDA, 0.87 GGA.

We know that the micro hardness parameter provides well estimation about the elastic and permanent plastic deformations of the compounds. And formulated as in Chen et. al. (41) micro hardness empirical model:

$$H_\upsilon = 2(K^2G)^{0.585} - 3 \qquad (22)$$

and Louie formulation (38):

$$H_\upsilon = 0.92\ K^{1.137}\ G^{0.708} \qquad (23)$$

In this study, the the micro hardness parameter is found 23.1, 32.4 (LDA) and 23.0, 29.5 (GGA) for Chen and Louie formulations respectively.

The Debye temperature, θ_D, is one of the distinctive characteristics of solid crystal structure that is connected to various physical properties (spatially elastic constants), its material can be making it possible to compute the Debye temperature as (42):

$$\theta_D = \frac{h}{k}\left[\frac{3n}{4\pi}\frac{N_A\rho}{M}\right]^{1/3} \cdot V_m \qquad (24)$$

here V_m is average velocity of sound, h shows the Planck's constant, k illustrates the Boltzmann's constant, N_A denotes Avogadro's number, n is related to number of atoms in unit cell when M points out the molecular weight and ρ density.

When we compare the Debye temperatures for GGA and LDA calculations in this study, we found that they differ somewhat. As shown in the table, LDA (902.7 K) is higher than GGA (867.3 K). Our GGA results (894.6 K) are comparable to the Ref. (8). The Debye temperature of MgB_2 is given as 1026.7 K (37). CaB_2 has a considerably lower Debye temperature than MgB_2, indicating that MgB_2 is more tightly bonded, and harder than CaB_2.

3.4 Electronic Band Structures and Fermi Surface Topologies

The electronic band structure and partial density of states are computed in this study for the compound CaB_2, at the theoretically defined equilibrium geometry as in Fig. 3.9 and Fig. 3.10. The SC features of this kind of materials are widely known to be caused by the large density of *d* states around the Fermi level (43). The features of Fermi surface are also important for determining the superconducting properties of the compounds (44).

The band structures clearly show metallicity for the CaB_2 compound. There is no crucial difference between the two calculated band structures for LDA and GGA. The valance bands, which start at -10 eV levels, consist of the *s* levels of Boron atoms. As clearly seen in the figures, there are three Fermi level crossing bands that mostly consist of B-atoms *p* state and Ca-atoms *d* states. As we

mentioned before, *d* levels are important in determining the superconductivity properties of such materials (43).

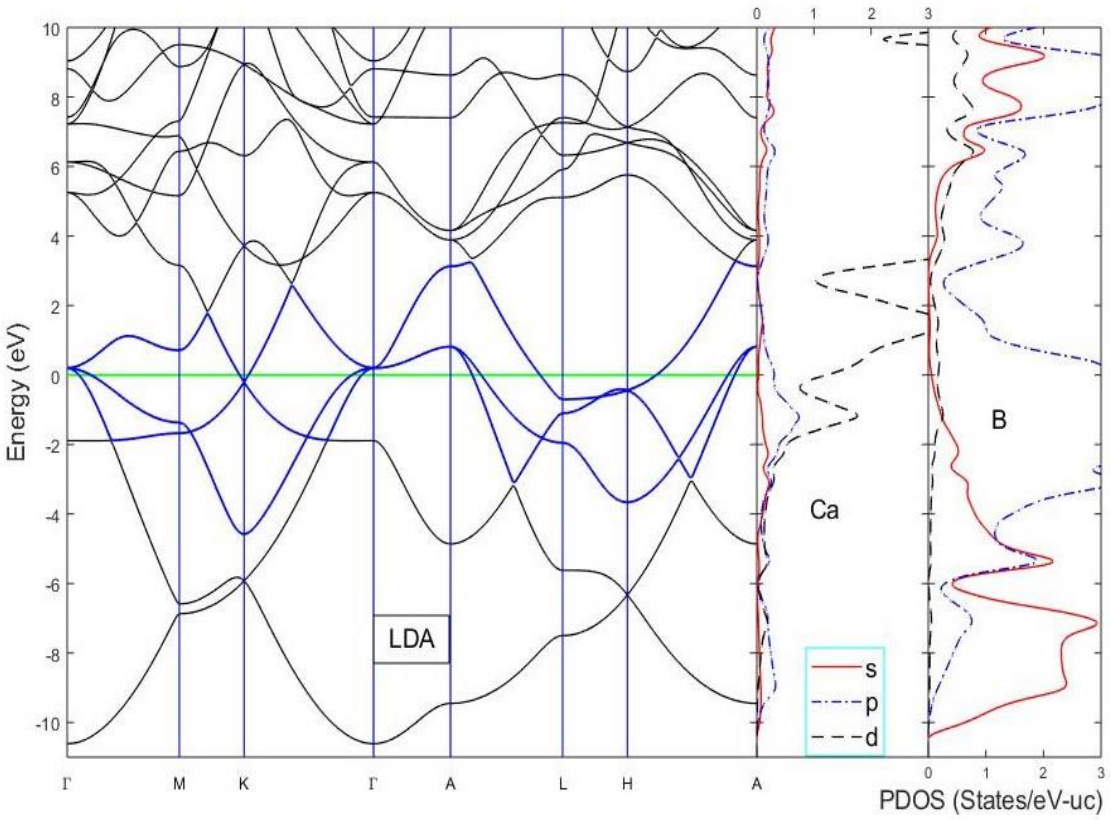

Figure 3.9. CaB_2 partial DOS and electronic band structure (LDA).

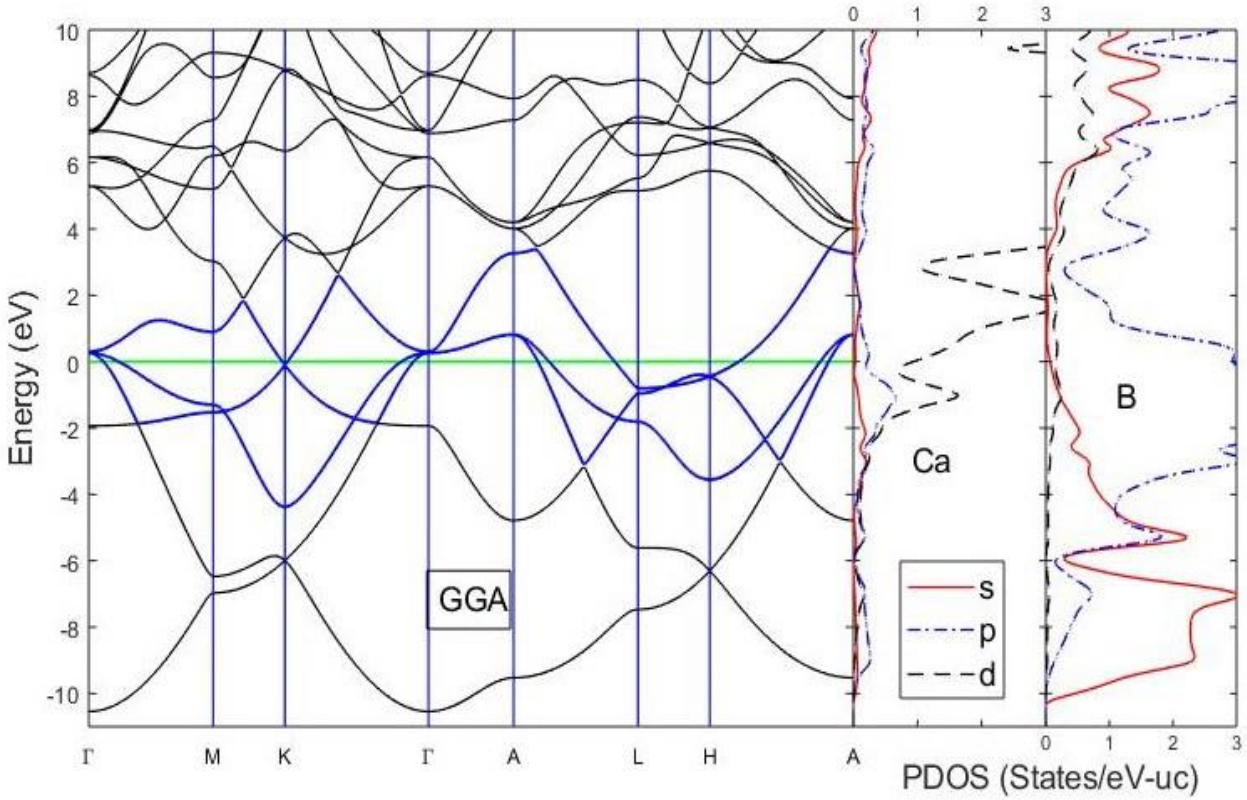

Figure 3.10. CaB_2 partial DOS as well as electronic band structure (GGA).

Previous first-principles calculations predicted that simplicity the hexagonal CaB_2 must have a unit cell with greater values of *a* and *c*. Also, according to first-principle calculations, the simple hexagonal CaB_2 should have a much larger value for the density of states at the fermi energy (E_F) than MgB_2. Both these features are because CaB_2 has higher T_C value than MgB_2 (31).

CaB_2 is an attractive candidate for superconductivity. But it has not yet been synthesized, nor has it been synthesized on a large scale. It has been studied theoretically for SC. Electronic structure of CaB_2 polymorphs exhibits well-localized peaks compared to superconducting MgB_2 because of the small lattice constant of MgB_2.

The electronic properties of MgB_2 are related to the 2*p* metallic states of B atoms in planar lattices, which determines the DOS near the E_F (30). As in MgB_2, the Fermi energy in CaB_2 is below top of σ-bands, creating two hole-type cylindrical sheets along the Γ−A line. While the hole-type sheets are qualitatively

close to those of MgB_2, the electron-type sheet of the π-bands in CaB_2 is quite different in MgB_2, the π bands are higher than the E_F at points M and K, however, in CaB_2, they are lower than E_F. Thus, CaB_2 has a single electron-type Fermi surface of the bands along the H lines. H – L, and Fermi surface is lost along the K−L line present in MgB_2.

The result of strong coupling between the electron and the phonon and Ref. (30), explained the behavior of *px* and *y*-band holes in negatively charged boron planes. Where Ref. (45) confirm an important role for B metal states in the appearance of SC as a whole.

The Fermi surface in CaB_2 consists of three sheets: two hole-type cylindrical ones along Γ−A lines and one electron-type along H–L lines. The DOS at the Fermi level in CaB_2 is 0.96 states/eV, which is much larger than 0.69 states/eV for MgB_2 (7). The last descriptor reveals that the large difference between the critical transition temperatures for the SC phenomenon can partially be explained by the electronic properties and Fermi surface topology due to lack of information about the phonon structure (21).

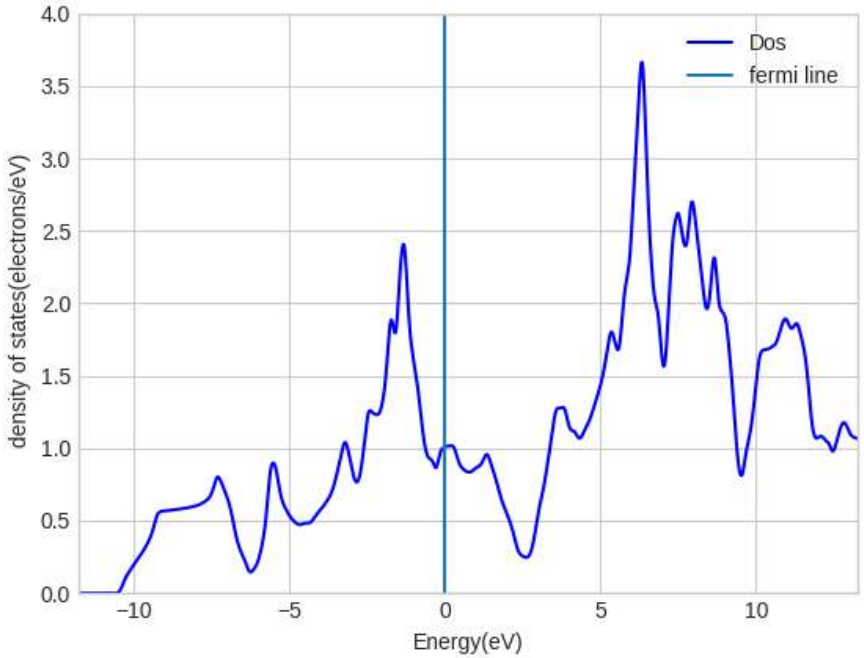

Figure 3.11. Total DOS CaB_2 (LDA).

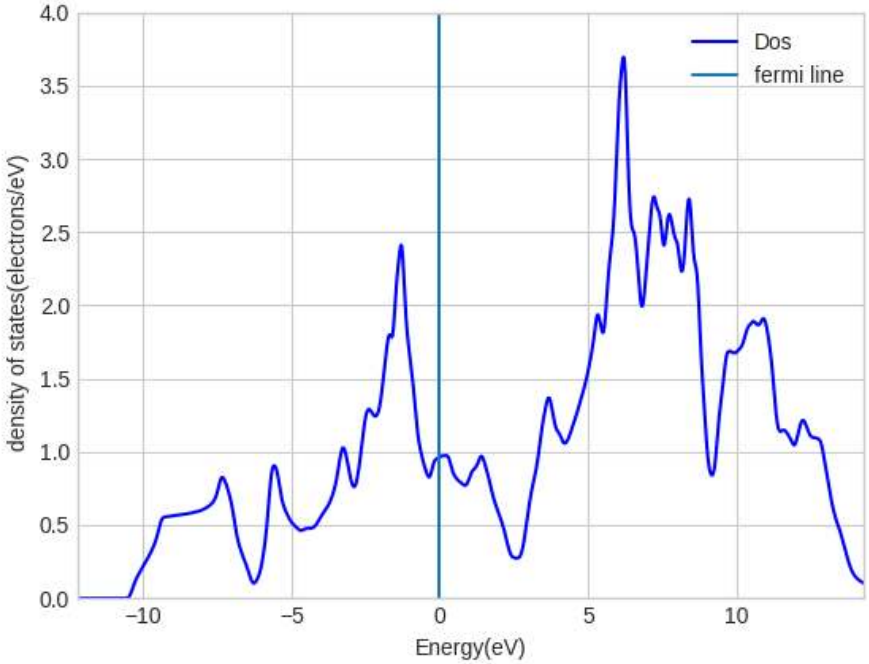

Figure 3.12. Total DOS CaB_2 (GGA).

As can be seen in Fig.3.11 and Fig.3.12 total densities of states at the Fermi level 0.971 (GGA) and 1.016 (LDA) states·eV^{-1}. cell^{-1}, mostly consist of Ca-d and B-p states as mentioned before and this value reported in Ref (7). as 0.96 similar with results. These levels important for SC properties as they may be due to the high DOS at Fermi level (43).

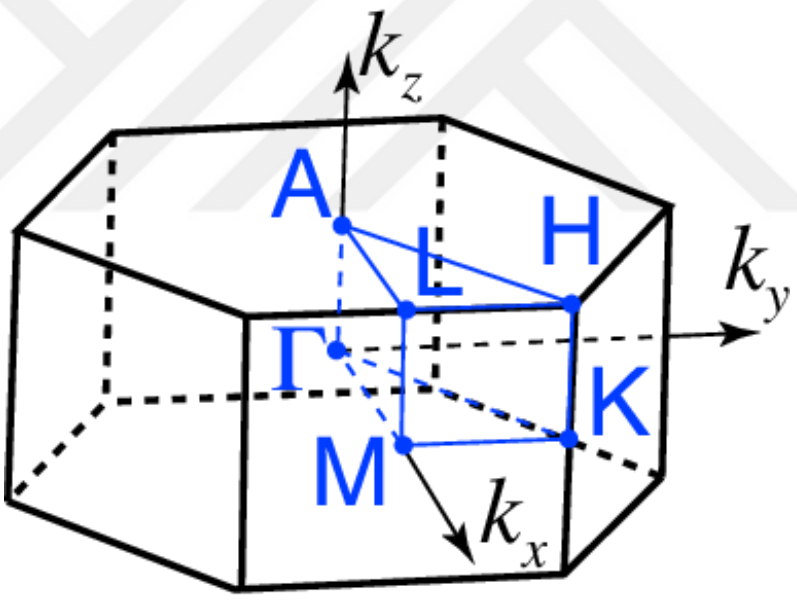

Figure 3.13. High symmetry point of the hexagonal stuctures Brillouin zone (46).

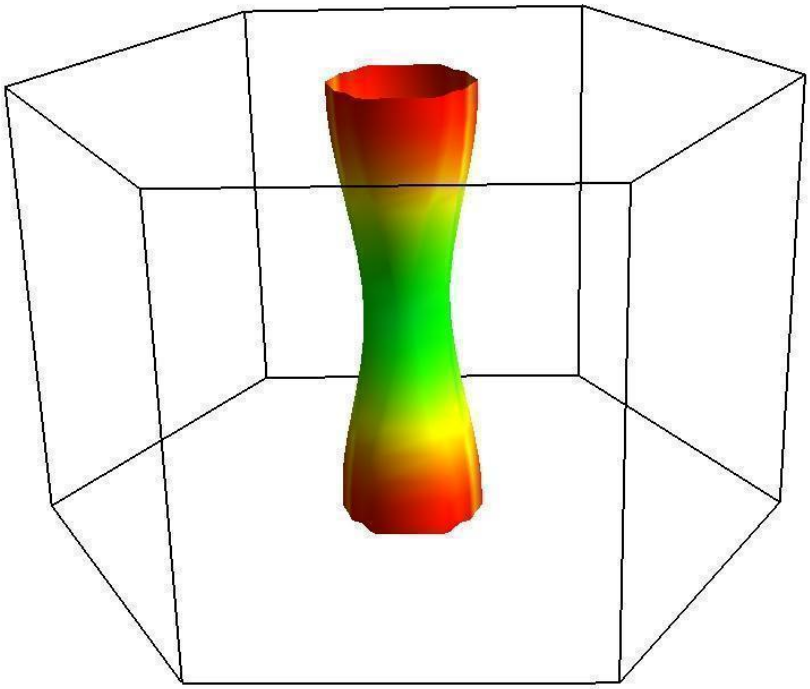

Figure 3.14. Fermi surface contribution of Fermi level crossing 7th band.

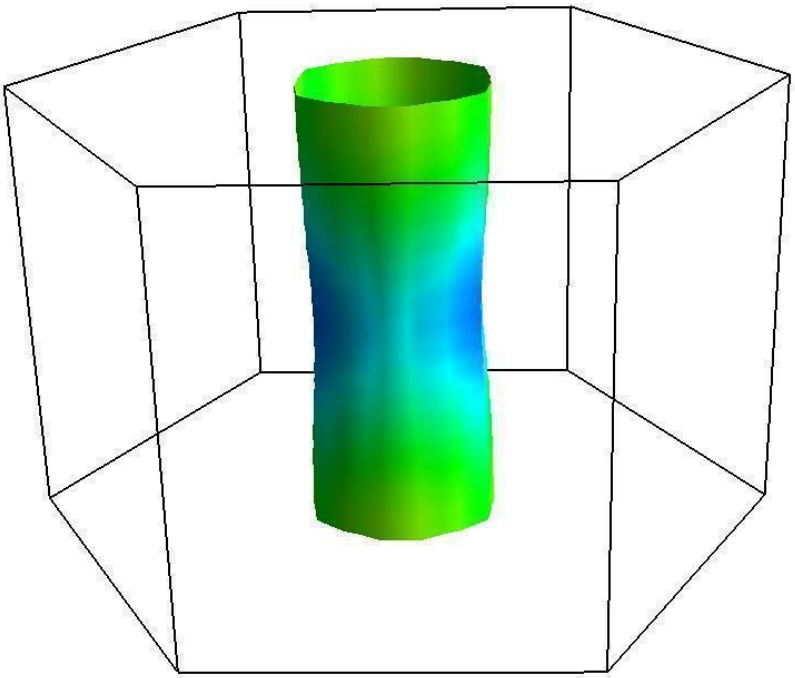

Figure 3.15. Fermi surface contribution of Fermi level crossing 8th band.

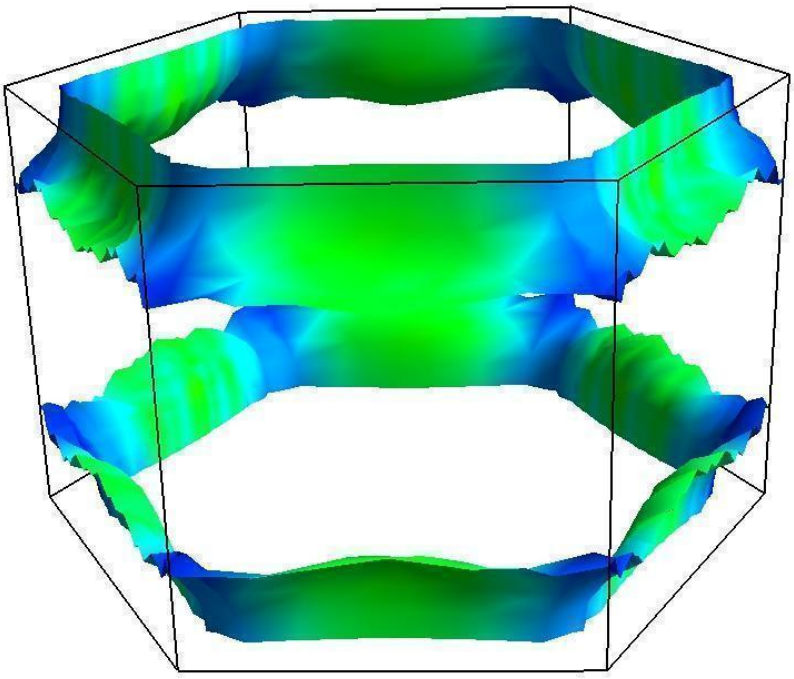

Figure 3.16. Fermi surface contributions of Fermi level crossing 9th band.

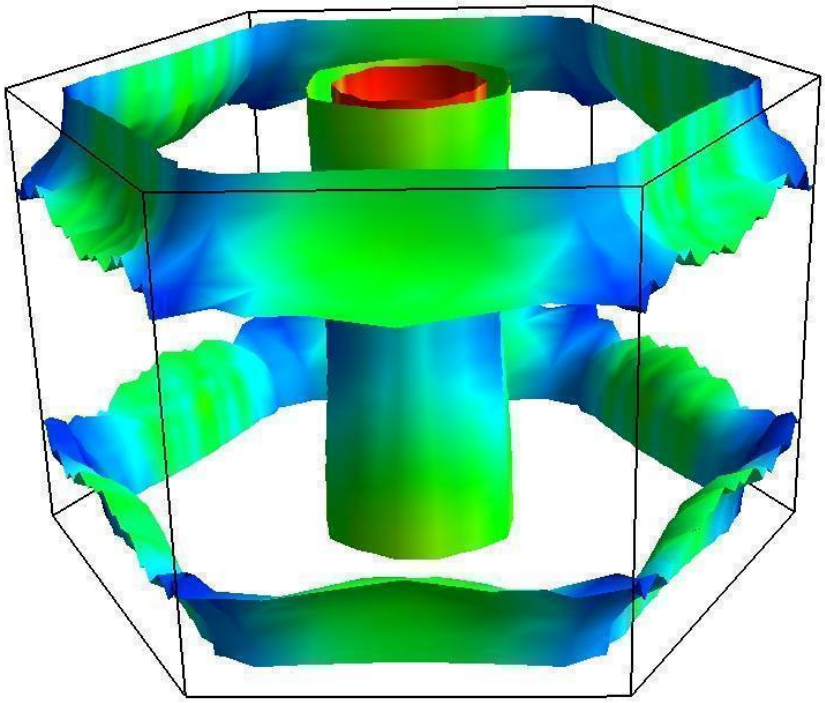

Figure 3.17. Complete Fermi surface structure of CaB_2.

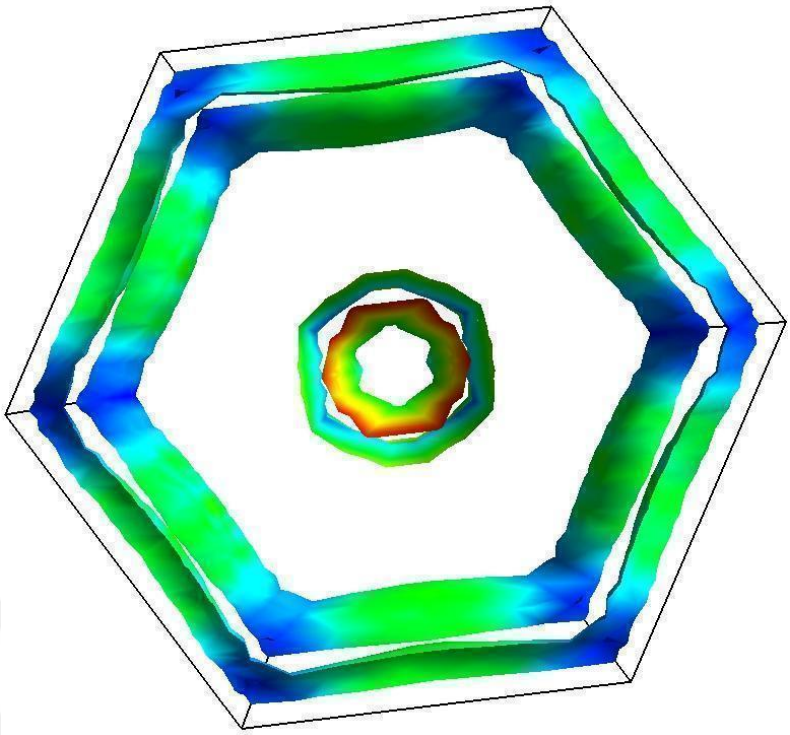

Figure 3.18. Complete Fermi surface structure of CaB_2 in top view.

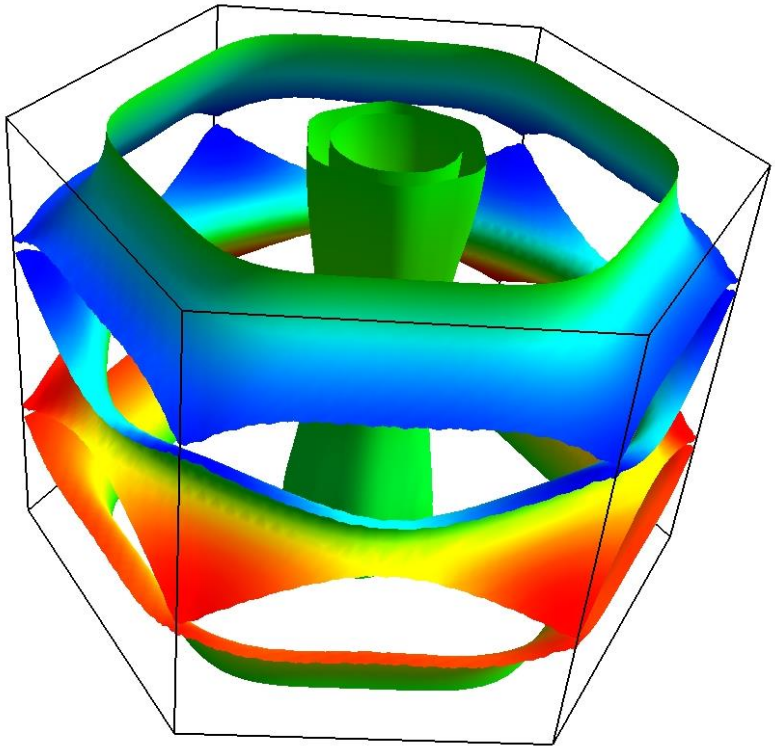

Figure 3.19. Complete Fermi surface structure of MgB_2 (47).

We use the optimized lattice constants to do first-principles calculations on the electrical structure. Illustrates the high-symmetry lines and resultant band structure at the Fermi surface. Overall, the CaB_2 band structure is similar to that of MgB_2. The bands are caused by the boron sp^2 and p_Z orbitals, respectively. Due to the greater B-B bond length than in MgB_2, total band width of bands is much lower. Due to its lower Fermi energy, CaB_2 displays two cylindrical hole-type sheets along its bands, just like MgB_2. Although the hole-type sheets from the CaB_2 bands are qualitatively quite different from those from MgB_2, the electron-type sheets are qualitatively identical.

Even though the hole-type sheets from the CaB_2 bands are significantly compared to those from MgB_2, the electron-type sheet from the bands in CaB_2 is very dissimilar from that in MgB_2. Because in MgB_2, the π bands are above fermi energy E_F at K and M points. Yet, those bands are below the fermi energy in CaB_2 at the same points. For the reasons mentioned above, the CaB_2 has only one electron-type fermi surface from the π bands together with H-L lines, lacking the MgB2 Fermi surface along the K-L line. So, to be concluded, CaB_2 contain three sheets in its fermi surface: two hole-type cylindrical sheets along Γ-A lines and just one electron-type along H-L lines. Compared to MgB_2, which has a density of 0.69 states.$eV^{-1} \cdot cell^{-1}$, CaB_2 has a substantially higher density of 0.96 states.$eV^{-1} \cdot cell^{-1}$ (7).

On the Fermi surface of MgB_2, there are two cylindrical plates in the region Γ, and it also has plates on top that are skirt-like in composition in the region L-H and the paintings of the same type in the same area L-H, but upside down. This is quite like the compound CaB_2. The difference between the two compounds is that the MgB_2 complex contains plates in the middle of the six sides in the M-K region and the CaB_2 complex does not contain these plates.

3.5 Vibrational and Superconducting Properties

A phonon defined to mediate the SC in a metal Intercalating superconductor, electron-phonon coupling (epc) is the implied cause of superconductivity. For that reason, the studying of phonon modes is an important tool for understanding the superconductivity mechanism of such materials. For that reason, the detailed phonon structure of CaB_2 is calculated in both Exc.s GGA and LDA. For phonon frequency, we use DFPT.

Knowing that the CaB_2 is belonging to the space group P6/mmm which have the irreducible representation at the vicinity of Brillouin zone center as

$$B_{1g} \oplus A_{2g} \oplus A_{2u} \oplus E_{2g} \oplus E_{1u} \oplus E_{1g}$$

where A_{2g} and E_{1g} are related to the acoustic modes. The calculated phonon frequencies for CaB_2 are shown in Table-3.8.

Table 3.8. Phonon frequencies in cm $^{-1}$ at center of the Brillouin Zone.

Mode	Pre.Work (LDA)	Pre.Work (GGA)	(8)	(7)	(31)
B_{1g}	392.4	372.9	390.8	416.7	
A_{2u}	286.7	277.4	277.0	290.3	305
E_{1u}	395.3	365.8	286.2		263
E_{2g}	657.6	644.2	647.9	658.6	588

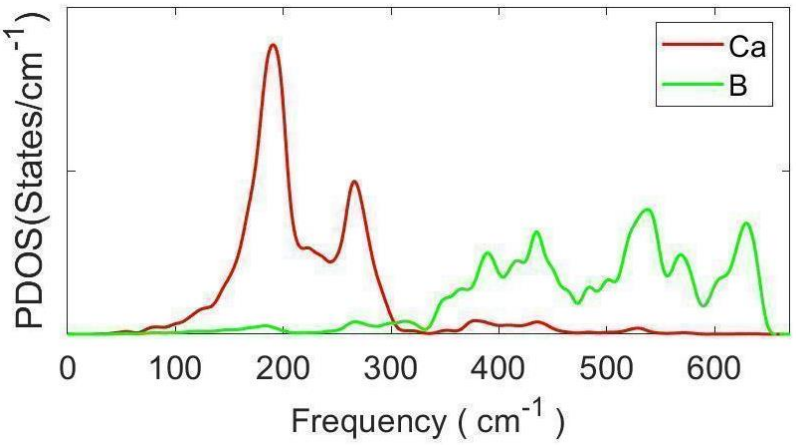

Figure 3.20. Partial phonon density of state of CaB_2 (GGA)

This little differentiation between calculations may be related to use different methods in the calculations. Probably all calculations use different types of pseudopotentials in mentioned that table.

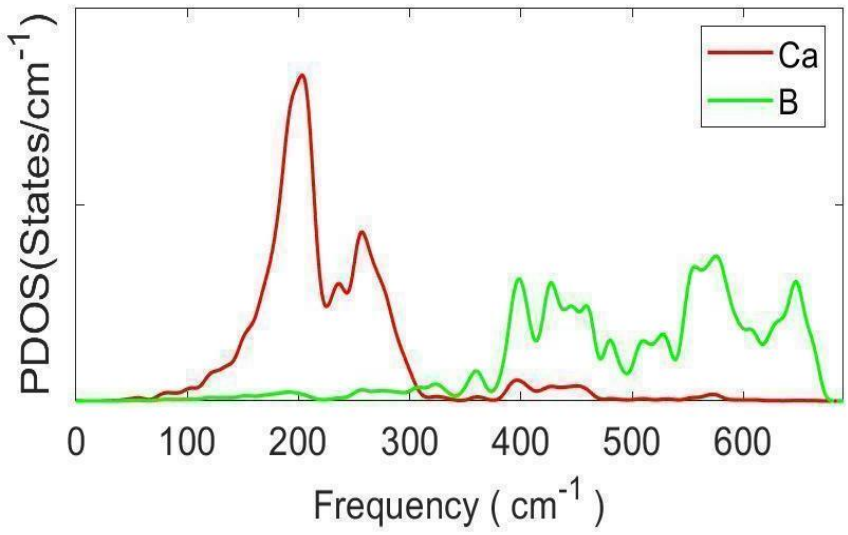

Figure 3.21. Partial phonon density of state of CaB_2 (LDA).

The phonon density of states DOS of CaB_2 can be seen in Fig.3.20 for GGA and Fig.3.21 for LDA. These exhibit no negative modes at zero pressure, demonstrating a compound's dynamical stability. Furthermore, both figures show that the vibrational regions between 100 cm^{-1} and 300 cm^{-1} are mostly brought on by vibrations of Ca atoms. Based on vibrations of B atoms, the phonon frequency bands for GGA and LDA are around 330 cm^{-1} to 660 cm^{-1} and 380 cm^{-1} to 680 cm^{-1}, respectively.

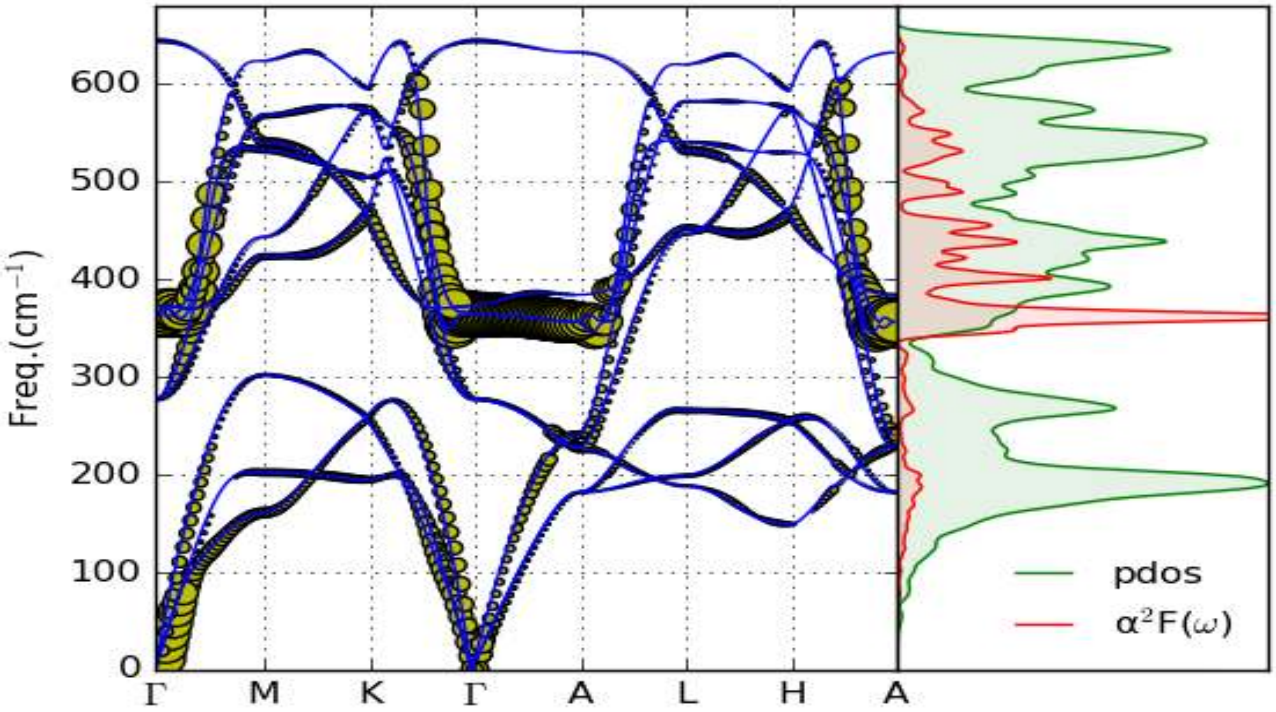

Figure 3.22. Phonon spectrum of CaB_2 in cm^{-1} (left). The size of each blue circle is proportional to the magnitude of electron-phonon coupling strength (λ_{qv}). The Phonon DOS (green-filled area (states/cm^{-1})) and the Eliashberg function $\alpha^2F(\omega)$ (red filled area) in arbitrary unit (GGA-Exc.).

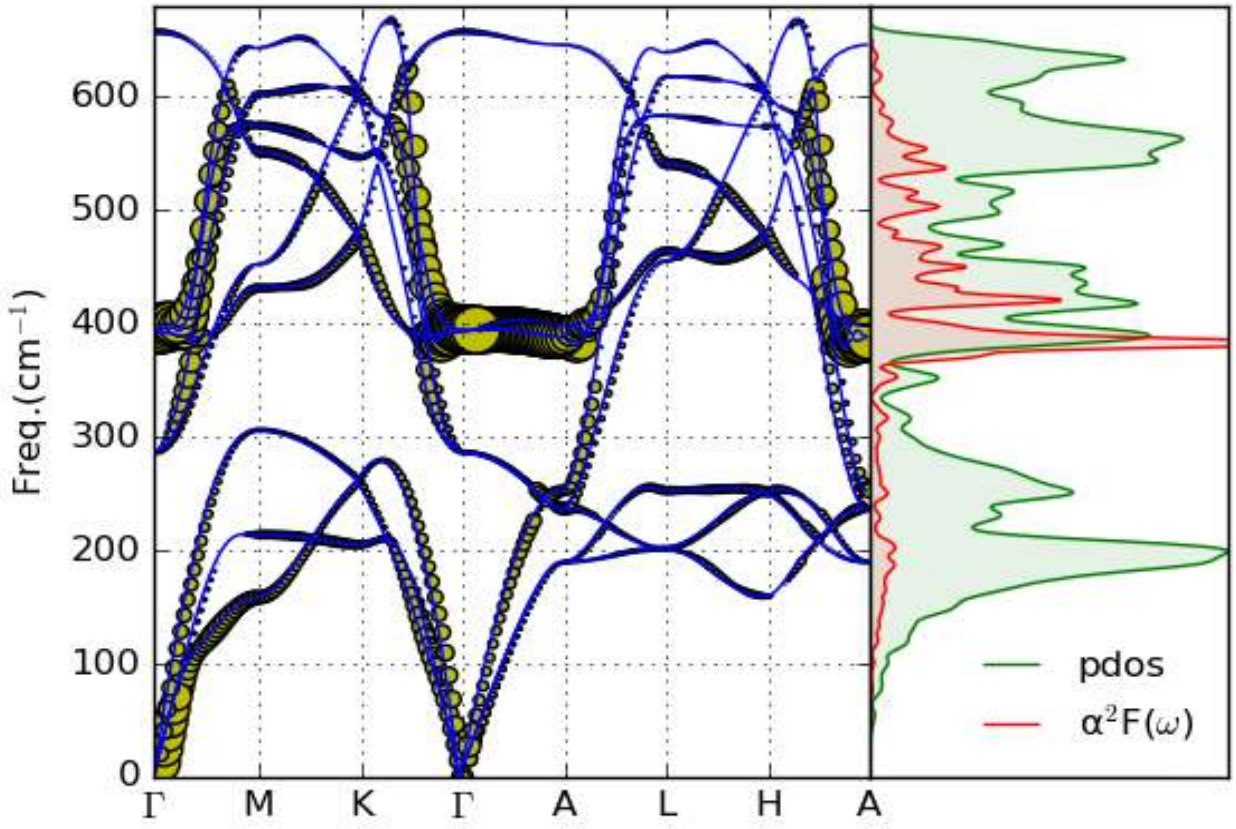

Figure 3.23. Phonon spectrum of CaB_2 in cm^{-1} (left). The size of each blue circle is proportional to the magnitude of electron-phonon coupling strength ($\lambda_{q\upsilon}$). The Phonon DOS (green-filled area (states/cm^{-1})) and the Eliashberg function $\alpha^2F(\omega)$ (red filled area) in arbitrary unit (LDA-Exc.).

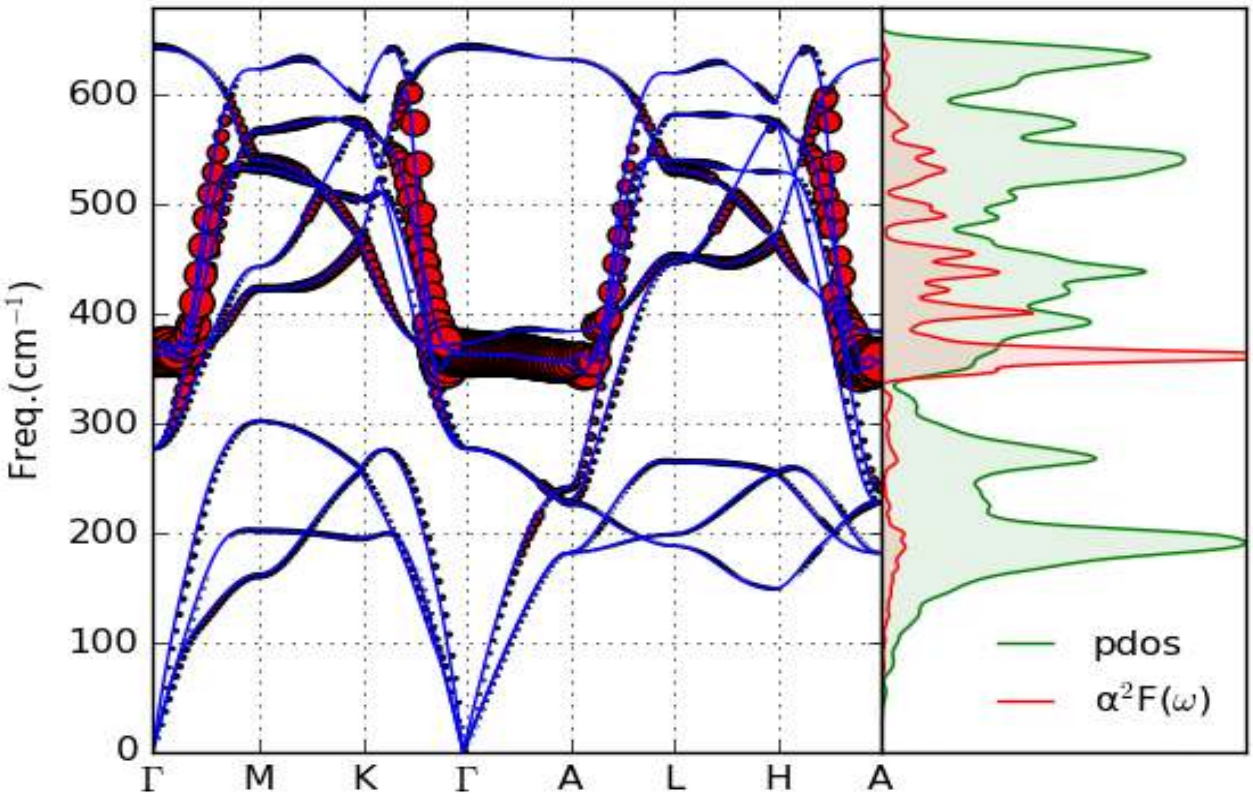

Figure 3.24: Phonon spectrum of CaB_2 in cm^{-1} (left). Red circles indicate the phonon linewidth ($\gamma_{q\upsilon}$) with a radius proportional to the strength. The Phonon DOS (green-filled area (states/cm^{-1}) and the Eliashberg function $\alpha^2F(\omega)$ (green-filled area) in arbitrary units (GGA-Exc.).

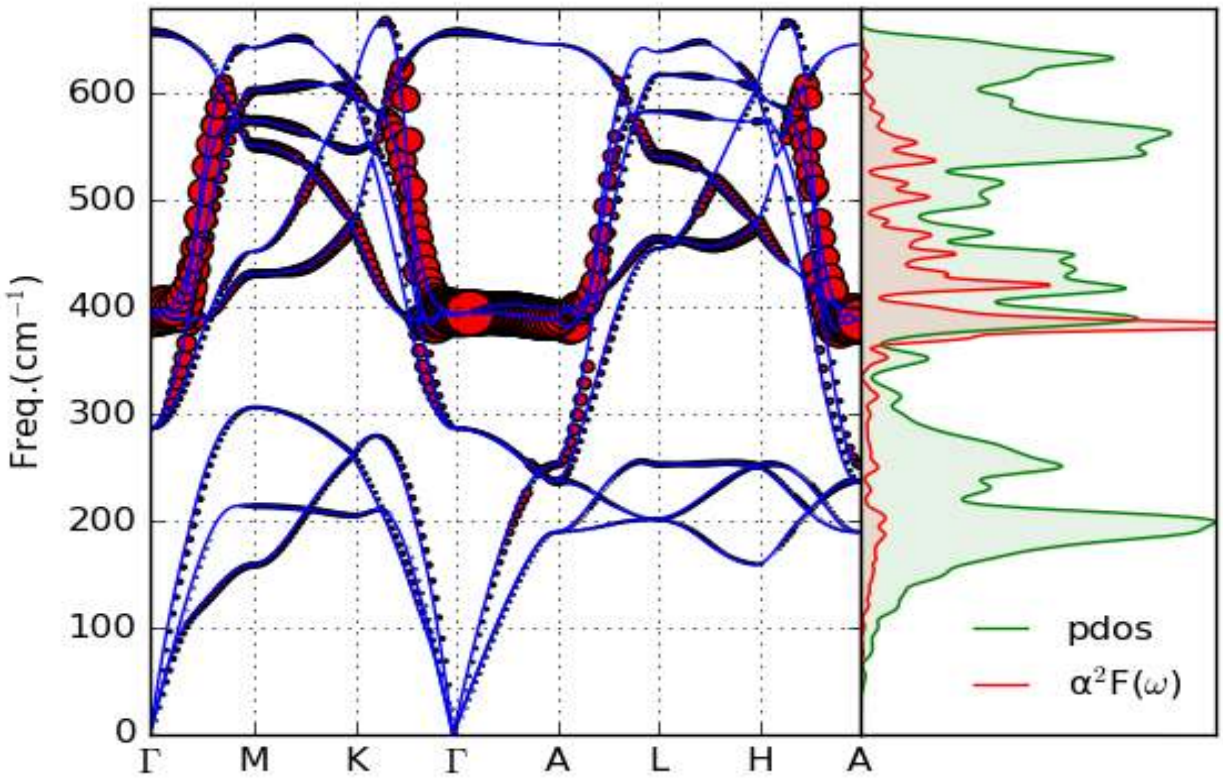

Figure 3.25. Phonon spectrum of CaB_2 in cm^{-1} (left). Red circles indicate the phonon linewidth ($\gamma_{q\upsilon}$) with a radius proportional to the strength. The Phonon DOS (green-filled area (states/cm^{-1}) and the Eliashberg function $\alpha^2F(\omega)$ (green-filled area) in arbitrary units (LDA-Exc.)

The phonon dispersion curve supply important information about the dynamical properties of materials (Fig.3.22-Fig.3.25). So many materials' physical characteristics, including specific heat, thermal expansion, free energy, heat conduction, sound velocity, and electron-phonon coupling, are dependent on their phonon properties. Moreover, imaginary frequencies indicate that the computed structure is not the most stable one, whereas low-frequency modes might be connected to phase changes.

We have calculated the phonon spectrums for CaB_2 with the density of states and Eliashberg spectra function in GGA and LDA. The results of our calculations on the phonon dispersive curve show that CaB_2 in the AlB_2 structure is a dynamically stable compound again. This stability in CaB_2 modes goes to the fact that its phonon dispersion curves do not contain soft modes at any wave vector

and all phonon frequencies at the high symmetry points are positive, so, they do not show structural instability (8).

The superconducting transition temperature T_C has been calculated using Allen-Dynes modified McMillen equation Through Eq. (5)-(6), and (7). Taking the value for $\mu^* = 0.1$ in our calculations, the obtained T_C value is 24.71 K for GGA and 22.75 K for LDA, and the logarithmic average frequency (ω_{ln}) for CaB_2 equals 475.48 K (GGA) and 0.793 K (LDA). Also, the isotropic λ is calculated to be 0.843 (GGA) and 0.793 (LDA) as given in Table 3.9.

Table 3.9. The calculated electron-phonon coupling constant (λ), the logarithmic averaged frequency (ω_{ln} in K), Debye temperature (Θ_D in K), total densities of states at Fermi level ($N(E_F)$ in states·eV^{-1}.$cell^{-1}$) and superconducting transition temperature (T_C in K).

Material	λ	ω_{ln}	Θ_D	T_C	$N(E_F)$	Ref
CaB_2	0.843	475.48	867.348	24.71	0.971	Pre.work μ*=0.1 (GGA)
CaB_2	0.793	493.28	902.771	22.75	1.016	Pre.work μ*=0.1 (LDA)
CaB_2	0.69	580.2		50.46	0.96	Ref. (7) μ*=0.10, 0.14
CaB_2	0.75			9.4~28.6		Ref. (48) μ*=0.14
MgB_2	0.73	706.7		40		Ref. (21) μ*=0.05
AlB_2	0.43	579.1		9		Ref. (49) μ*=0.05
MgC_2	0.62	594.2	717.96	14.9		Ref. (50) μ*=0.1

By comparing our results with the other results in Table 3.9, it was found that the value of the electron-phonon coupling constant (λ), highest values in our results were 0.843 (GGA) and 0.793 (LDA), followed by the Yu Z. et. al. (48) a value of (0.75), the lowest value mentioned in for the Ref. (7) is 0.69 for CaB_2, but as mentioned in the table the value of MgB_2 (0.73) in the Ref. (21), which is a result close to the results of CaB_2.

The value found in our calculations for the compound CaB_2 Debye temperature Θ_D is 902.771 K (LDA), followed by 876,348 K (GGA). Compared Θ_D with the compound MgC_2, for the Ref (50), the value Θ_D (717.69 K) It's less than our results. As expected from this situation, the T_C of MgC_2 is much lower than that of CaB_2.

When we compare the T_C value of CaB_2 we calculated with the T_C value calculated for MgB_2, it is clearly seen that the T_C value of CaB_2 is low. This does not match the values calculated. (7). The reason for this is probably different from the method used by Choi *et.al*. (7). However, it is seen in the same table that the value we calculated is very compatible with the recent study (48).

The highest logarithmic mean frequency (ω_{ln}) value for CaB_2 is for Ref. (7) (580.2 K) as followed in our calculations by 493.28 K (LDA), as well as 475.48 K (GGA) for the same compound. The highest logarithmic value of the compound MgB_2 which is 706.7 K and is higher than our calculated results. As mentioned in the Ref. (49) for the compound AlB_2, which is equal to 579.1 K and is the lowest value in Table 3.9 (In addition, we can consider that the value of λ is very lowfor AlB_2.).

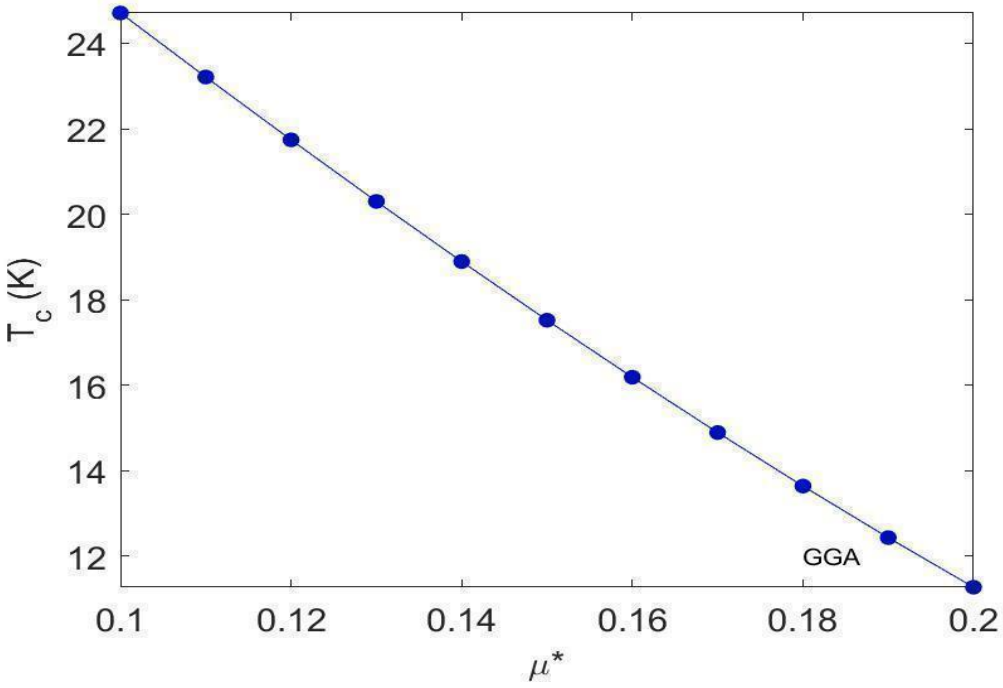

Figure 3.26. The critical temperature T_C as a function of μ* for GGA.

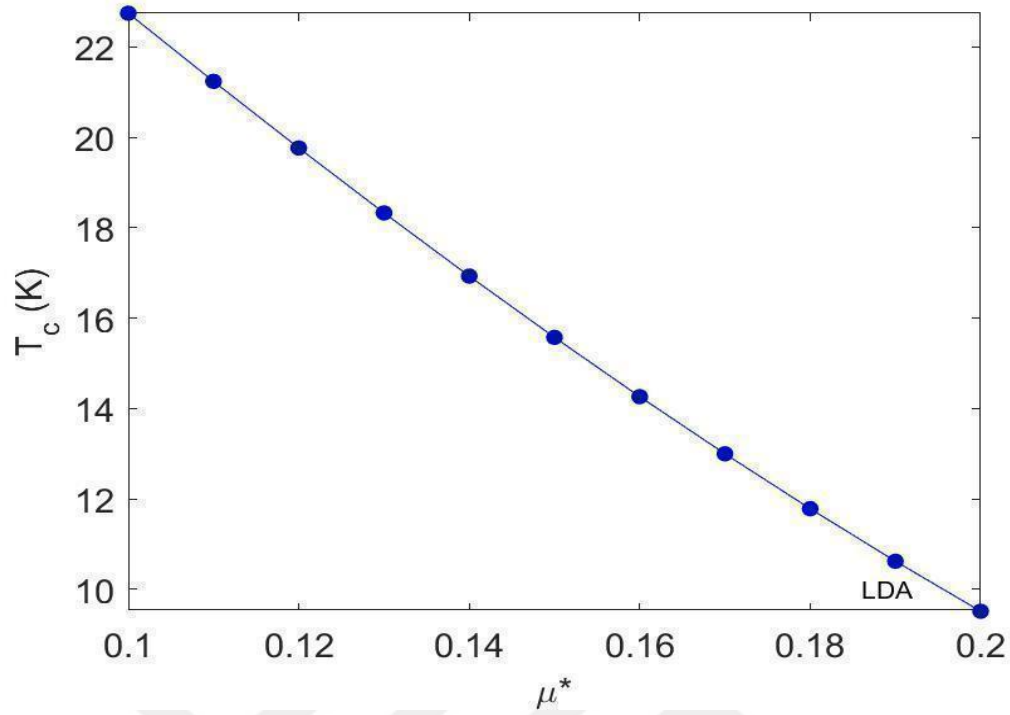

Figure 3.27. The critical temperature T_C as a function of μ* for LDA.

According to the results obtained, it can be concluded that the λ directly affects the critical transition temperatures. For this reason, the higher λ the material exhibits the larger the transition temperature it obtains. The low-lying phonon branch plays an active role in relatively higher T_C and λ values (21). Also as encountered in Eq. (1), the ω_{ln} is directly proportional to T_C. Besides, as can be clearly seen from the phonon distribution graphs (Fig.3.22-Fig.3.25), the electron-phonon coupling strength ($\lambda_{q\upsilon}$) and phonon line width ($\gamma_{q\upsilon}$) are very concentrated around 400 cm^{-1}, which shows us that the electron-phonon interaction is very dominant in these regions.

Figures 3.26 and Figures 3.27 show us how the superconducting transition temperature changes with the coulomb potential (μ*). And as expected, these two quantities move in inverse propotional.

4. CONCLUSION

In this thesis, we have studied calculations on the physical properties of CaB_2 in the AlB_2 structure by using first principles techniques with GGA and LDA exchange correlations, and norm-conserving pseudopotentials with a plane wave basis set.

We calculate detailed, lattice structure properties as lattice constants, bond lengths, and Bulk modulus of the material. With the aid of the DFPT, we get elastic constants, phonon frequencies, and epc properties which are crucial for SC properties. We found that the electronic band structures, electron density of states, and fermi surface topologies. The related mechanical properties like shear modulus, Young's modulus, Poisson's ratio, Debye temperature, and shear anisotropic factors are calculated and discussed.

CaB_2 structure is the mechanically stable compound in AlB_2 structure, because the material obeys the Born stability criteria and dynamically stable compound, due to there is not the existing of the imaginary phonon frequencies. Our calculation shows that CaB2 is a high T_C SC, due to our calculated T_C values being 24.71 K, 22.75 K for GGA and LDA Exc. respectively. These values are like the recent study of Ref. (47) (28.6 K) but different from Ref. (7) (50,46 K) result. We explained this different result as the consideration of anharmonic phonon interactions in the related study (7).

Our research has led us to the conclusion CaB_2 is brittle in AlB_2 phase. A material's brittleness is closely related to Pugh's modulus (G/B), the crucial value of which is G/B>0.5. The Pugh's ratio of CaB_2 found for the materials is 0.84 LDA and 0.87 GGA. The value found in our calculations for the compound CaB_2 Debye temperature (Θ_D) is (902.771 K) LDA, followed by (876,348 K) GGA. Related to the combination of high Debye temperature and strong electron–phonon coupling constant values, the materials require to exhibit a relatively high T_C value.

We found that the Fermi surface topologies of CaB_2 are similar to MgB_2 Fermi surface topologies, just difference between the two compounds is that the MgB_2 complex contains plates in the middle of the six sides in the M-K region and the CaB_2 complex does not contain these plates. Our calculations have shown total densities of states (DOS) at the Fermi levels 0.971 (GGA) and 1.016 (LDA) states·$eV^{-1\cdot}$ $cell^{-1}$, mostly consisting of Ca-d and B-p states, and this value is similarly reported in Ref. (7) as 0.96 states·$eV^{-1\cdot}$ $cell^{-1}$.

We hope that this thesis will soon help to conduct a practical experiment to find the compound CaB_2 and lead to the study of more binary compounds in AlB_2 phase that may have superconductivity.

5. REFERENCE

Vancouver citation system was used on this thesis

1. Uber die Darstellung und die Eigenschaften von. 1969;434(1954):1969.

2. Ravindran P, Vajeeston P, Vidya R, Kjekshus A, Fjellvåg H. Detailed electronic structure studies on superconducting (formula presented) and related compounds. Phys Rev B - Condens Matter Mater Phys. 2001;64(22):1–15.

3. Kuroiwa S, Saura Y, Akimitsu J, Hiraishi M, Miyazaki M, Satoh KH, et al. Multigap superconductivity in sesquicarbides $La2C_3$ and Y_2C_3. Phys Rev Lett [Internet]. 2008 Mar 6 [cited 2022 Sep 7];100(9):097002. Available from: https://journals.aps.org/prl/abstract/10.1103/PhysRevLett.100.097002

4. Parlak C. The physical properties of AlB2-type structures $CaGa_2$ and $BaGa_2$: An ab-initio study. Phys B Condens Matter. 2020 Jan 1;576.

5. Vinod K, Abhilash Kumar RG, Syamaprasad U. Prospects for MgB_2 superconductors for magnet application. Supercond Sci Technol. 2007;20(1).

6. Boeri L, Bachelet GB. Viewpoint: The road to room-temperature conventional superconductivity. J Phys Condens Matter. 2019;31(23):1–9.

7. Choi HJ, Louie SG, Cohen ML. Prediction of superconducting properties of CaB_2 using anisotropic Eliashberg theory. Phys Rev B - Condens Matter Mater Phys. 2009;80(6):80–3.

8. Ozisik HB, Colakoglu K, Deligoz E. Crystal structures, elastic, and lattice dynamical properties of BeB_2, NaB_2, and CaB_2 from the first principles. J Phys Chem Solids. 2012 Apr;73(4):593–8.

9. Shein IR, Ivanovskii AL. Elastic properties of mono-and polycrystalline hexagonal AlB_2-like diborides of s, p and d metals from first-principles calculations. J Phys Condens Matter. 2008;20(41).

10. Kawamura M. FermiSurfer: Fermi-surface viewer providing multiple representation schemes. Comput Phys Commun. 2019 Jun 1;239:197–203.

11. Dal Corso A. Density-functional theory beyond the pseudopotential local density approach : a few cases studies. Sissa. 1993;(October).

12. Parlak C. Elastic, electronic, lattice dynamical properties and electron-phonon interaction in the ternary superconductors Ba(GaGe) and Ba(GaSi). Comput Mater Sci. 2015 Feb 1;96(PA):360–4.

13. Snider E, Dasenbrock-Gammon N, McBride R, Debessai M, Vindana H, Vencatasamy K, et al. Room-temperature superconductivity in a carbonaceous sulfur hydride. Nature [Internet]. 2020;586(7829):373–7. Available from: http://dx.doi.org/10.1038/s41586-020-2801-z

14. Botana AS, Norman MR. Similarities and Differences between $LaNiO_2$ and $CaCuO_2$ and Implications for Superconductivity. Vol. 10, Physical Review X. 2020.

15. Pokluda J, Černý M, Šob M, Umeno Y. Ab initio calculations of mechanical properties: Methods and applications. Prog Mater Sci. 2015;73:127–58.

16. Feynman RP. PARTONS. 1983 Jan;329–424.

17. Sauer T, Grebogi C, Yorke JA. How Long Do Numerical Chaotic Solutions Remain Valid? Phys Rev Lett [Internet]. 1997 Jul 7 [cited 2022 Sep 5];79(1):59. Available from: https://journals.aps.org/prl/abstract/10.1103/PhysRevLett.79.59

18. Burke K, Perdew JP, Wang Y. Derivation of a Generalized Gradient Approximation: The PW91 Density Functional. Electron Density Funct Theory. 1998;81–111.

19. Cihan Parlak, First Principle investigation of lattice dynamical properties of CU-Based chalcopyrite semiconductors and high dielectric constant materials. PhD thesis (March) 2008.

20. Payne C, York N. Iterative minimization techniques for ab initio total-energy molecular dynamics and conjugate gradients calculations : 1992;64(4).

21. Parlak C. Elastic, electronic, lattice dynamical properties and electron-phonon interaction in the ternary superconductors Sr(GaGe) and Sr(GaSi) at high pressure. Phys B Condens Matter [Internet]. 2017 Sep 15 [cited 2021 Oct 31];521(April):251–7. Available from: http://dx.doi.org/10.1016/j.physb.2017.06.077

22. Schwerdtfeger P. The Pseudopotential Approximation in Electronic Structure Theory. ChemPhysChem [Internet]. 2011 Dec 9 [cited 2022 Sep 5];12(17):3143–55. Available from: https://onlinelibrary.wiley.com/doi/full/10.1002/cphc.201100387

23. Abdul Majeed Aamar, Structural and electronic properties of some Hessler compounds, Master thesis 28/09/2020.

24. Gonze X, Beuken JM, Caracas R, Detraux F, Fuchs M, Rignanese GM, et al. First-principles computation of material properties: The ABINIT software project. Comput Mater Sci. 2002;25(3):478–92.

25. --Opium-- Pseudopotential generation project [Internet]. [cited 2022 Sep 6]. Available from: http://opium.sourceforge.net/

26. van Setten MJ, Giantomassi M, Bousquet E, Verstraete MJ, Hamann DR, Gonze X, et al. The PSEUDODOJO: Training and grading a 85 element optimized norm-conserving pseudopotential table. Comput Phys Commun. 2018;226:39–54.

27. Viswanathan E, Sundareswari M, Jayalakshmi DS, Manjula M. Fermi surface and hardness enhancement study on ternary scandium and vanadium based borides by first principles investigation. Comput Mater Sci [Internet].

2019;157(October 2018):107–20. Available from: https://doi.org/10.1016/j.commatsci.2018.10.040

28. Oguchi T. Cohesion in AlB_2-Type Diborides: A First-Principles Study. J Phys Soc Japan. 2002 Jun;71(6):1495–500.

29. De Jong M, Chen W, Angsten T, Jain A, Notestine R, Gamst A, et al. Charting the complete elastic properties of inorganic crystalline compounds. Sci Data. 2015 Mar 17;2.

30. Okatov S V, Ivanovskii AL, Medvedeva YE, Medvedeva NI. The Electronic Band Structures of Superconducting MgB_2 and Related Borides CaB_2 , MgB_6 and CaB_6. 2001;5(1):44–6.

31. Vajeeston P, Ravindran P, Fjellvåg H. Prediction of structural, lattice dynamical, and mechanical properties of CaB_2. RSC Adv. 2012;2(31):11687–94.

32. Parlak C. Theoretical investigation of superconductivity in Ba(AlSn) under pressure. Phys C Supercond its Appl [Internet]. 2016 Oct 15;529:21–5. Available from: http://dx.doi.org/10.1016/j.physc.2016.08.008

33. Duan YH, Sun Y, Guo ZZ, Peng MJ, Zhu PX, He JH. Elastic constants of AlB2-type compounds from first-principles calculations. Comput Mater Sci. 2012;51(1):112–6.

34. Woolley JC. Introduction to solid state physics. Vol. 6, Journal of the Mechanics and Physics of Solids. 1957. 83 p.

35. Waller I. Dynamical Theory of Crystal Lattices by M. Born and K. Huang . Acta Crystallogr. 1956;9(10):837–8.

36. Hill R. The Elastic Behaviour of a Crystalline Aggregate. Proc Phys Soc Sect A [Internet]. 1952 May 1 [cited 2022 Sep 6];65(5):349. Available from: https://iopscience.iop.org/article/10.1088/0370-1298/65/5/307

37. Li Y, Hao J, Liu H, Tse JS, Wang Y, Ma Y. Pressure-stabilized superconductive yttrium hydrides. Sci Rep. 2015;5:1–8.

38. Tian Y, Xu B, Zhao Z. Microscopic theory of hardness and design of novel superhard crystals. Int J Refract Met Hard Mater. 2012 Jul 1;33:93–106.

39. Ranganathan SI, Ostoja-Starzewski M. Universal elastic anisotropy index. Phys Rev Lett. 2008;101(5):3–6.

40. Ding H, Dwaraknath SS, Garten L, Ndione P, Ginley D, Persson KA. Computational Approach for Epitaxial Polymorph Stabilization through Substrate Selection. ACS Appl Mater Interfaces. 2016 May 25;8(20):13086–93.

41. Zhao C, Zhou C, Chen C. Preparation and characterization of BiFeO3/La0.7Sr0.3MnO3 heterostructure grown on SrTiO3 substrate. Phys B Condens Matter [Internet]. 2017;521(July):376–80. Available from: http://dx.doi.org/10.1016/j.physb.2017.06.078

42. Equations of State for Solids in Geophysics and Ceramic Science (Oxford Monographs on Geology and Geophysics) by Orson Anderson (1995-01-12): Amazon.com: Books [Internet]. [cited 2022 Sep 6]. Available from: https://www.amazon.com/Equations-Geophysics-Monographs-Anderson-1995-01-12/dp/B01K0TQVGW

43. Shein IR, Medvedeva NI, Ivanovskii AL. Band structure of new superconducting AlB_2-like ternary silicides M(Al0.5Si0.5)2 and M(Ga0.5Si0.5)2 (where M = Ca, Sr and Ba). J Phys Condens Matter. 2003;15(33):1–6.

44. Parlak C. First-principles study of the electronic structure and elastic properties of $SrGa_2$ under pressure. Mater Today Commun. 2021 Sep 1;28.

45. Kortus J, Mazin II, Belashchenko KD, Antropov VP, Boyer LL. Superconductivity of metallic Boron in MgB_2. Phys Rev Lett. 2001;86(20):4656–9.

46. Yuan H, Bahramy MS, Morimoto K, Wu S, Nomura K, Yang BJ, et al. Zeeman-type spin splitting controlled by an electric field. Nat Phys. 2013;9(9):563–9.

47. FermiSurfer Web page [Internet]. [cited 2022 Sep 6]. Available from: https://fermisurfer.osdn.jp/

48. Yu Z, Bo T, Liu B, Fu Z, Wang H, Xu S, et al. Superconductive materials with MgB_2-like structures from data-driven screening. 2022;2. Available from: https://arxiv.org/abs/2202.11355v1

49. Capelle K. A bird's-eye view of density-functional theory. Brazilian J Phys. 2006;36(4 A):1318–41.

50. Kuroda K, Ochi M, Suzuki HS, Hirayama M, Nakayama M, Noguchi R, et al. Experimental Determination of the Topological Phase Diagram in Cerium Monopnictides. Phys Rev Lett. 2018 Feb 21;120(8).